Molecular Pharmacology Fast Forward. Published on November 7, 2018 as DOI: 10.1124/mol.118.113159
This article has not been copyedited and formatted. The final version may differ from this version.

Title Page: Subcellular Localization and Activity of the Mitogen-activated Protein Kinase Kinase 7 (MKK7) γ Isoform are Regulated through Binding to the Phosphatase Calcineurin*

Authors: Emily S. Gibson, Kevin M. Woolfrey, Huiming Li, Patrick G. Hogan, Raphael A. Nemenoff, Lynn E. Heasley, and Mark L. Dell'Acqua†

Affiliations: ESG, KMW, MLD: Department of Pharmacology, University of Colorado School of Medicine, Anschutz Medical Campus, Aurora, CO, USA 80045

RAN: Department of Medicine, Division of Renal Diseases and Hypertension, University of Colorado School of Medicine, Anschutz Medical Campus, Aurora, CO, USA 80045

LEH: Department of Craniofacial Biology, University of Colorado School of Dental Medicine, Anschutz Medical Campus, Aurora, CO, USA 80045

HL: Immune Disease Institute, Harvard Medical School, Boston, MA, USA. Current address: Acceleron Pharma, 128 Sidney Street, Cambridge, MA 02139.

PGH: La Jolla Institute for Allergy & Immunology, La Jolla, CA, USA.

Molecular Pharmacology Fast Forward. Published on November 7, 2018 as DOI: 10.1124/mol.118.113159
This article has not been copyedited and formatted. The final version may differ from this version.

Running Title Page: MKK7γ interaction with calcineurin

Corresponding Author:

Mark L. Dell'Acqua

Department of Pharmacology,

University of Colorado School of Medicine

Anschutz Medical Campus

12800 E. 19th Ave, Mail Stop 8303

Aurora, CO 80045.

Tel: 303-724-3616.

Fax: 303-724-3663

Email: mark.dellacqua@ucdenver.edu

Text pages: 38

Figures: 10

References: 38

Abstract: 236 words

Introduction: 643 words

Discussion: 1263 words

Abbreviations: AKAP, A-kinase anchoring protein; AVP, Arginine-Vasopressin; BLASTP, basic local-alignment sequence tools-protein; BSA, bovine serum albumin; CaN, calcineurin/protein phosphatase 2B; c-FLIP$_L$, cellular FLICE-inhibitory protein; CsA, cyclosporine A; CFP, cyan-fluorescent protein; FRET, fluorescence resonance energy transfer; GFP, green-fluorescent protein; JNK, c-Jun N-terminal kinase; MKK7, mitogen-activated protein kinase kinase 7; NFAT, Nuclear factor of activated T cells; PBS, phosphate-buffered saline; PKA, cAMP-dependent protein kinase; PKC, protein kinase C; rVSMC, rat vascular smooth muscle cells; YFP, yellow-fluorescent protein.

Molecular Pharmacology Fast Forward. Published on November 7, 2018 as DOI: 10.1124/mol.118.113159
This article has not been copyedited and formatted. The final version may differ from this version.

Abstract

Calcineurin (CaN) phosphatase signaling is regulated by targeting CaN to substrates, inhibitors, and scaffold proteins containing docking motifs with the consensus sequence of PxIxIT. Here, we identify docking of CaN to the γ isoform of MKK7, a component of the c-Jun N-terminal kinase (JNK) pathway. Due to alternative splicing of a single exon within the N-terminal domain, MKK7γ encodes a unique PxIxIT motif (PIIVIT) that is not present in MKK7 α or β. We found that MKK7γ bound directly to CaN through this PIIVIT motif *in vitro*, immunoprecipitated with CaN from cell extracts, and exhibited fluorescence resonance energy transfer (FRET) with CaN in the cytoplasm but not the nucleus of living cells. In contrast, MKK7α and β exhibited no direct binding or FRET with CaN and were localized more in the nucleus than the cytoplasm. Furthermore, inhibition of CaN phosphatase activity increased the basal phosphorylation of MKK7γ but not β. Deletion of the MKK7γ PIIVIT motif eliminated FRET with CaN and promoted MKK7γ redistribution to the nucleus; however, inhibition of CaN activity did not alter MKK7γ localization, indicating that MKK7γ cytoplasmic retention by CaN is phosphatase activity-independent. Finally, inhibition of CaN phosphatase activity in vascular smooth muscle cells, which express MKK7γ mRNA, enhances JNK activation. Overall, we conclude that the MKK7γ-specific PxIxIT motif promotes high-affinity CaN binding that could promote novel crosstalk between CaN and JNK signaling by limiting MKK7γ phosphorylation and restricting its localization to the cytoplasm.

Molecular Pharmacology Fast Forward. Published on November 7, 2018 as DOI: 10.1124/mol.118.113159
This article has not been copyedited and formatted. The final version may differ from this version.

Introduction

The ubiquitous phospho-ser/thr protein phosphatase CaN (also known as PP2B and PPP3) controls many important cellular functions, including the immune response in T cells, hypertrophic growth of myocytes, and synaptic plasticity in neurons. Elevations in intracellular Ca^{2+} stimulate the phosphatase activity of the CaN A catalytic subunit through Ca^{2+} binding to a pre-associated CaN B regulatory subunit and to calmodulin, which binds adjacent to CaNB subunit on the CaN A subunit C-terminal regulatory domain. The concerted actions of Ca^{2+}-CaNB and Ca^{2+}-CaM then cause a conformational change in the CaNA regulatory domain that leads to displacement of an auto-inhibitory domain from the catalytic active site (Li *et al.*, 2011). However, the CaNA subunit also engages in additional protein-protein interactions with a variety of binding partners that contain docking motifs with the consensus sequence of PxIxIT. These diverse CaN-PxIxIT docking interactions can in turn regulate the specificity of CaN signaling by controlling substrate recognition, catalytic activity, and subcellular targeting to multi-protein signaling complexes by scaffold proteins (Aramburu *et al.*, 1998; Grigoriu *et al.*, 2013; Li *et al.*, 2011; Murphy *et al.*, 2014; Oliveria *et al.*, 2007; Sanderson *et al.*, 2012).

The PxIxIT docking motif was originally identified in studies that characterized the mechanism by which CaN first recognizes and then dephosphorylates the Nuclear Factor of Activated T cells (NFAT) family of transcription factors to promote NFAT translocation from the cytoplasm to the nucleus to control gene expression (Aramburu *et al.*, 1998). Subsequent peptide library screening identified the PVIVIT peptide as an artificial PxIxIT motif with sub-micromolar CaN binding affinity (Aramburu *et al.*, 1999). X-ray crystallographic determination of the structure of the PVIVIT-CaN complex elucidated the molecular basis CaN A subunit binding to PxIxIT motifs through a β-sheet interaction at a site distant from the phosphatase catalytic site, thus explaining how PxIxIT binding can direct either active or inactive CaN to specific substrates (Li *et al.*, 2007). Interestingly, there is considerable non-consensus variation in the PxIxIT motif sequences for different CaN binding proteins, leading to wide range of binding

Molecular Pharmacology Fast Forward. Published on November 7, 2018 as DOI: 10.1124/mol.118.113159
This article has not been copyedited and formatted. The final version may differ from this version.

affinities, with K_d values from sub-micromolar to hundreds of micromolar (Goldman *et al.*, 2014; Li *et al.*, 2011). For instance, our recent X-ray structure-function analysis of the postsynaptic plasma membrane scaffold protein A-kinase anchoring protein (AKAP) 79 identified an IAIIIT variant of this motif that interacts with CaN at the same site as PVIVIT but with Ile substituting for Pro in the first position (Li *et al.*, 2012). However, this AKAP79 non-consensus variant motif binds CaN with sub-micromolar affinity, which is similar to PVIVIT and actually greater than all other known naturally occurring consensus PxIxIT sequences.

An important feature of AKAP79 is that it not only binds CaN to target it to specific substrates but also anchors two opposing protein kinases, the cAMP-dependent protein kinase (PKA) and the Ca^{2+} and phospholipid activated protein kinase C (PKC), thus, allowing for coordinated bi-directional regulation of phosphorylation and integration of different second messenger pathways within a single signaling complex (Wild and Dell'Acqua, 2018; Woolfrey and Dell'Acqua, 2015). Based on the AKAP79-CaN/PKA/PKC scaffold model, we sought to identify other signaling proteins that could anchor CaN and protein kinases in the same signaling complex. To this end, we used a combination of *in silico*, biochemical, and cellular imaging approaches to identify and characterize a consensus PxIxIT CaN docking motif in the γ isoform splice variant of the mitogen-activated protein (MAP) kinase, kinase 7 (MKK7; also known as MAPKK7), a key upstream kinase regulator of JNK signaling. In particular, we demonstrate that this PxIxIT motif promotes high-affinity CaN binding to MKK7γ, selectively regulates MKK7γ phosphorylation, and restricts localization of MKK7γ to the cytoplasm instead of the nucleus, where the related MKK7α and β isoforms lacking this motif are concentrated. Importantly, we also provide evidence that this scaffolding of CaN to MKK7γ may promote crosstalk between CaN and JNK signaling in vascular smooth cells.

Molecular Pharmacology Fast Forward. Published on November 7, 2018 as DOI: 10.1124/mol.118.113159
This article has not been copyedited and formatted. The final version may differ from this version.

Materials and Methods

cDNA Expression Plasmids and Transfection of HEK-293 and COS7 cells: Previous publications describe plasmids encoding CaNAα-myc (Dell'Acqua *et al.*, 2002), CaNAα-CFP/YFP (Oliveria *et al.*, 2003), CaNAαH151A-YFP (Oliveria *et al.*, 2012), PVIVIT-GFP (Aramburu *et al.*, 1999), and Flag-MKK7α1, β1 and γ1 isoforms (Tournier *et al.*, 1999). N-terminally tagged YFP and CFP versions of MKK7α1, β1 and γ1 were constructed by transfer of Flag-MKK7 encoding HindIII-XbaI fragments into pEC/YFPC1 (Clontech). The ΔPIX mutation deleting residues 41PIIVIT46 in MKK7γ1 was introduced by Quick-change PCR (Stratagene). HEK-293 and COS7 cells at 20-50% confluency (24-48 hrs after plating) were transfected by calcium phosphate precipitation with the various plasmid cDNA expression constructs (1-2 μg each plasmid per 25 mm glass coverslip in six-well plates for FRET imaging or 2-10 μg each plasmid for 10 cm plates for immunoprecipitation) for 4-6 hours at 5% CO_2, 37°C. Cells were then washed with phosphate buffered saline (PBS), fed with normal growth medium (Dulbecco's Modified Eagle Medium (DMEM), 10% Fetal Bovine Serum, 1% penicillin/streptomycin, Invitrogen) and grown 24-48 hours prior to fluorescence imaging or preparation of cell extracts for immunoprecipitation.

Immunoprecipitation of CaN-MKK7 Complexes from HEK-293 Cell Extracts: We analyzed Flag-MKK7 and CaNA-myc binding by co-immunoprecipitation (co-IP) from transfected HEK-293 cell extracts essentially as described for AKAP79 binding to CaNA-myc (Dell'Acqua *et al.*, 2002). In Figure 8, cells were treated with 1 μM ionomycin (Tocris) for 3 min prior to co-IP. Briefly, HEK-293 cells on 10 cm dishes were washed twice in PBS prior to harvesting. Cell extracts were prepared by lysis in ice cold buffer containing 0.5% Triton X-100 (TLB: 20 mM Hepes pH 7.4, 100 mM NaCl, 5 mM EDTA, 0.5 % TX-100 (w/v), 1 mM DTT, 2 mg/ml leupeptin/pepstatin, 1 mM Benzamidine, 1 mM AEBSF) followed by clarification of the lysate by centrifugation at 16,000xg for 15 min. Approximately 1.0 mg of cell lysate was

Molecular Pharmacology Fast Forward. Published on November 7, 2018 as DOI: 10.1124/mol.118.113159
This article has not been copyedited and formatted. The final version may differ from this version.

incubated at 4°C overnight with 2 μg of either mouse anti-myc (9E10; Santa Cruz), rabbit anti-Flag (sc-807; Santa Cruz), or unrelated mouse or rabbit non-immune IgG. After antibody incubations, protein A-sepharose (Pierce) (25 μl, 50% slurry equilibrated in TLB) was added and incubated for 1 hour at 4°C. The immunecomplexes were pelleted by microcentrifugation (3,000 x g, 1 minute) and the beads washed in TLB (4 x 1 ml). The immunecomplexes were eluted with SDS-PAGE sample buffer, separated by SDS-PAGE and transferred to nitrocellulose filters. Filters were analyzed by immunoblotting with anti-Flag (1:1000), anti-myc (1:1000) or rabbit anti-GFP (1:500; Invitrogen) and horse-radish peroxidase-coupled secondary antibodies (Bio-Rad). Immunoblots were then visualized using enhanced chemiluminescence (Pierce) and a Fluor-chem gel documentation system (Alpha Innotech).

Immunoprecipitation of MKK7 species for phosphorylation analysis was done as previously described (Woolfrey *et al.*, 2015) with modifications as detailed below: HEK-293FT cells were transfected with myc-CaN and YFP-MKK7β1 or YFP-MKK7γ1 by calcium phosphate precipitation as above. Cells were then treated with CaN inhibitors cyclosporin A (2 μM) and FK-506 (2 μM) (Tocris) for 30 minutes, rinsed in PBS + 1 mM Ca^{2+}, and lysed in ice cold RIPA buffer plus inhibitors (20 mM Tris, pH7.4, 150 mm NaCl, 1% Triton X-100, 1% NP-40, 5 mM EDTA, 5 mM NaF, 5 mM β-Glycerophosphate, 2 mg/ml leupeptin, 2 mg/ml pepstatin, and 1 mM 4-(2-aminoethyl)benzenesulfonyl fluoride). After pelleting cell debris, 5% of each sample was set aside for input and the remaining lysate was tumbled overnight at 4°C with anti-GFP antibody (4 μg, A-11122, Life Technologies). The following day, lysates were tumbled with protein A sepharose beads (Pierce) for 2 hours at 4°C. Following 3 washes with lysis buffer, protein was eluted from beads in 2X sample buffer + DTT (50 μM). Samples were then resolved using SDS-PAGE and western blotting for phosho-MKK7 (#4171, Cell Signaling, 1:1000 in 5% BSA TBS-T), anti-GFP (1:1000) and anti-myc (1:100).

Molecular Pharmacology Fast Forward. Published on November 7, 2018 as DOI: 10.1124/mol.118.113159
This article has not been copyedited and formatted. The final version may differ from this version.

MKK7 Peptide-CaNA Binding Assays: N-biotinylated, C-amidated MKK7γ (35SPQRPRPIIVITLSPAPA52), MKKβ (35SPQRPRPTLQLPLANDGG52), PVIVIT (1GPHPVIVITGPHEE14) or control peptide (Ht31; 1LIEEAASRIVDAVIEQVK18) were custom synthesized (Biomatik). For precipitation of CaNA-myc from HEK-293 cell extracts, 10 μg of peptide was incubated with streptavidin-agarose (Sigma) (20 μl packed beads) in hypotonic buffer (10 mM Hepes, pH 7.4, 10 mM KCl, 1.5 mM $MgCl_2$, 0.1% Nonidet P40, 0.1% BSA, 1 mM DTT, 1 mM benzamidine, 1 mM leupeptin and 1 mM AEBSF) for 4 h at 4°C. The slurry was centrifuged (3000 x g) and the unbound peptide removed. The beads were then incubated with in ~1 mg of HEK-293 cell extracts expressing CaNA-myc in a total volume of 100 μl overnight at 4°C. Protein complexes were pelleted by centrifugation (3000 x g), washed 5x with hypotonic buffer containing 1 M NaCl and 5x with hypotonic buffer, eluted with SDS-PAGE sample buffer and immunoblotted using anti-myc as above. The ability of MKK7 and PVIVIT peptides to compete with fluorescent PVIVIT peptide for binding to purified calcineurin was measured as using fluorescence polarization as described (Li *et al.*, 2004). Briefly, a complex of 1 μM CaNA,B holoenzyme and 100nM Oregon green labeled PVIVIT was formed in PBS with 1mg/mL bovine gamma-globulin, followed by titration of MKK7γ peptide to 200 μM or MKK7β peptide to 2000 μM. Competition of fluorescence polarization representing Oregon-green-PVIVIT bound to CaN was measured using Synergy2 plate reader (BioTek).

Imaging of MKK7 and CaN Interaction and Localization in COS7 cells: Living COS7 cells on 25 mm glass coverslips were imaged at room temperature 24-48 hrs post-transfection using a Nikon TE-300 inverted microscope equipped with a 63x or 100x plan-apo/1.4NA objective, Chroma JP4 CFP/YFP/FRET filter sets, Sensicam digital CCD camera, and Slidebook 4.0 software (Intelligent Imaging Innovations). For three-filter (3F) micro-FRET measurements of sensitized FRET emission, CFP, YFP, and raw FRET images were captured with 2 x 2 binning. For measurements of FRET as CFP-donor dequenching after YFP-acceptor photobleaching

Molecular Pharmacology Fast Forward. Published on November 7, 2018 as DOI: 10.1124/mol.118.113159
This article has not been copyedited and formatted. The final version may differ from this version.

(PB), YFP was bleached in a subset of the same cells with 535 ± 20 nm light for 2 minutes and CFP imaged again essentially as described in (Gorski et al., 2005; Oliveria et al., 2007; Oliveria et al., 2003). Briefly, for the 3F FRET method, YFP, CFP and raw FRET fluorescence was detected in single xy planes in living cells using 250 ms exposure times to capture three images: 1) YFPexcitation/YFPemission 2) CFPexcitation/CFPemission and 3) CFPexcitation/YFPemission (raw FRET). After background subtraction, fractional image subtraction corrected for CFP bleed-through (0.5) and YFP cross-excitation (0.02) to yield an image of corrected, sensitized FRET (FRETc = raw FRET – (0.5*CFP) – (0.02*YFP), which was then gated to the CFP donor channel to create a FRETc/CFP pseudocolor image of relative FRET intensity in the cell. Mean CFP, YFP and raw FRET fluorescence intensities were then measured by mask analysis of cytoplasmic regions in Slidebook 4.0 as described previously (Oliveria *et al.*, 2007; Oliveria *et al.*, 2003; Sorkin *et al.*, 2000). Apparent FRET efficiency (Eeff) values for sensitized FRET were calculated from these mean intensities using the following equations as described in (Erickson *et al.*, 2003; Oliveria *et al.*, 2007): and Eeff=(FR-1)*(ε_{YFP440} / ε_{CFP440}), where FR=(rawFRET-(0.5*CFP))/(0.02*YFP) and ε_{YFP440} and ε_{CFP440} represent the average molar extinction coefficients for YFP and CFP over the band pass of the CFP excitation filter (ε_{YFP440} / ε_{CFP440} =0.094). For YFP PB measurements of CFP dequenching, Eeff was independently measured and calculated as Eeff=1-(CFPpre/CFPpost). Eeff calculated from either sensitized FRET measurements or PB measurements of CFP donor deqeunching takes into account cell-to-cell variation in expression of YFP and CFP, such that these FRET indices are effectively independent of donor and acceptor concentration. Similar mask analysis to measure mean CFP and YFP fluorescence intensity in regions of cytoplasm versus nucleus of individual living cells was performed to calculate the cytoplasm/nucleus mean intensity ratios presented in Figures 5 and 6. In Figure 7 COS7 cells were fixed in 3.7% formaldehyde in PBS

Molecular Pharmacology Fast Forward. Published on November 7, 2018 as DOI: 10.1124/mol.118.113159
This article has not been copyedited and formatted. The final version may differ from this version.

for 5 min prior to imaging CFP and YFP fluorescence and measurement of cytoplasm/nucleus mean intensity ratios as above for living cells.

RT-PCR Analysis of MKK7γ mRNA Expression: Total RNA (5 μg) was reverse transcribed in a volume of 20 μl using random hexamers and MMLV reverse transcriptase. Aliquots (1 μl) of reverse transcription reactions were subjected to PCR in 25 μl reactions with SYBR® green Jumpstart Taq Readymix (Sigma) and the primers for MKK7γ, forward primer 5'-ATCACTCTAAGCCCTGCTCC-3' and reverse primer 5'-TCTCTGAGGATGGTGAGCGG-3', using an I Cycler (BioRad). GAPDH mRNA levels were measured by quantitative RT-PCR with forward primer 5'-CGTGGAGTCTACTGGCGTCTTCAC-3' and reverse primer 5'-CGGAGATGATGACCCTTTTGGC-3' in replicate samples as for normalization of MKK7γ mRNA expression and the data are presented as "Relative Expression".

Phospho-JNK Immunoblots and JNK Activity Assays in Rat Vascular Smooth Muscle Cells: Rat vascular smooth muscle cells (rVSMC) cultured in Eagle's minimal essential medium (EMEM*)* containing 10% fetal bovine serum were switched to EMEM containing 0.2% fetal bovine serum and treated as indicated. Following incubation, the cell monolayers were rinsed with phosphate-buffered saline (PBS) and collected in lysis buffer (0.5% Triton X-100, 50 mM β-glycerophosphate (pH 7.2), 0.1 mM Na_3VO_4, 2 mM $MgCl_2$, 1 mM EGTA, 1 mM dithiothreitol, 2 mg/ml leupeptin and 4 mg/ml aprotinin). Microfuged extracts containing 200 μg of protein were submitted to immunoblot analyses for phospho-JNK1/2 (1:1000; Cell Signaling) or extracts were incubated (4 °C, 2 h) with 2 μg of anti-JNK1 antibody (C17; Santa Cruz) and 10 ml packed Protein A Sepharose in a total volume of 0.5 ml. The immune complexes were washed three times in lysis buffer and then suspended in 40 μl of 50 mM β-glycerophosphate (pH 7.2), 0.1 mM Na_3VO_4, 10 mM $MgCl_2$, 100 μM [g-^{32}P]-ATP (5000 cpm/pmol), 1 mM EGTA and 2 mg of GST-cJun(1-79). After a 20 min incubation at 30 °C, the kinase reactions were terminated with 10 μl of SDS sample buffer and submitted to SDS-PAGE. The GST-cJun(1-79) polypeptides

Molecular Pharmacology Fast Forward. Published on November 7, 2018 as DOI: 10.1124/mol.118.113159
This article has not been copyedited and formatted. The final version may differ from this version.

were excised from the Coomasie-stained and dried gels and incorporated radioactivity was determined in a scintillation counter.

Statistical Analyses: All graphs in the figures represent mean ± standard error and p values were determined as indicated in the figure legends by either unpaired, two-tailed Student's t-test in Excel for Mac 2011 version 14.7.7 (Microsoft), by one sample t-test in Prism version 4.0-6.0 (Graphpad), or by one-way ANOVA with Bonferroni's post-hoc correction for multiple comparisons in Prism version 4.0-6.0. A value of $p<0.05$ is considered significant unless otherwise noted in the figure legends due to additional adjustment for multiple comparisons.

Molecular Pharmacology Fast Forward. Published on November 7, 2018 as DOI: 10.1124/mol.118.113159
This article has not been copyedited and formatted. The final version may differ from this version.

Results

To identify novel signaling proteins that may bind CaN we used the program BLASTP (http://blast.ncbi.nlm.nih.gov) to search all non-redundant mouse, rat, and human protein sequences in GenBank, PDB, SwissProt, PIR and PRF for potential high-affinity PxIxIT motifs similar in sequence to PVIVIT or IAIIIT from AKAP79. The top hit in the search for sequences similar to PVIVIT identified residues 41PIIVIT46 in N-terminal domain of the γ isoform of MKK7 that conforms to a consensus PxIxIT motif and differs from PVIVIT by only a single substitution of I for V in the non-conserved second position (Figure 1A). Importantly, this 41PIIVIT46 sequence is identical in the MKK7γ sequences for humans, mice, and rats. The JNK MAPK pathway is activated by a number of different cellular stresses and receptors binding extracellular ligands (Figure 1B). In these pathways, MKK7 kinase activity is activated by Ser and Thr phosphorylation in its activation loop by a number of different upstream MAPKKKs and then activates JNK1/2/3 kinase activity through phosphorylation on Thr and Tyr residues in the JNK activation loop to then promote downstream phosphorylation of targets that control a variety of processes including transcription and apoptosis (Figure 1B)(Davies and Tournier, 2012). MKK7γ is one of three isoforms of MKK7 (α, β and γ) that differ in their N-terminal regions due to alternative splicing (Tournier *et al.*, 1999)(Figure 1C). The β and γ isoforms both possess an N-terminal regulatory domain (residues 1-91 in MKK7γ) appended to the kinase domain that contains docking sites for its downstream substrate/target JNK (Tournier *et al.*, 1999). In contrast, MKK7α lacks this N-terminal regulatory domain (Figure 1C). Closer inspection of the MKK7 gene structure reveals that the 41PIIVIT46 sequence is contained within a 17 amino acid region encoded by exon 2 that is unique to MKK7γ, thus MKK7β contains an alternatively spliced sequence in this region of 41PTLQLP46 which has, at best, weak homology to a PxIxIT motif, with only one consensus residue at P41, conservative substitutions of I for L at positions 43 and 45, and a non-conservative substitution of T for P at position 46 (Figure 1A). However,

Molecular Pharmacology Fast Forward. Published on November 7, 2018 as DOI: 10.1124/mol.118.113159
This article has not been copyedited and formatted. The final version may differ from this version.

as mentioned above, since there is considerable variation around the PxIxIT consensus motif in known CaN binding partners, both MKK7γ and β could potentially interact with CaN, albeit likely with different affinities.

To test for interactions between CaN and the different MKK7 isoforms, we transfected HEK-293 cells with C-terminal myc-tagged CaNA and N-terminal Flag-tagged MKK7 α, β, or γ and performed reciprocal co-immunpreciptation (co-IP) experiments (Figure 2A). There is also alternative splicing of the MKK7 C-terminal region generating a shorter and longer C-terminal version for each N-terminal variant (i.e. MKK7γ1 versus MKK7γ2; Figure 1C) giving rise to a total of 6 different MKK7 isoforms (Tournier *et al.*, 1999); however, we confined our analysis to the shorter α1, β1, and γ1 isoforms. Anti-Flag IP of MKKγ led to co-precipitation of CaNA-myc as predicted based on the presence of the strong, consensus PxIxIT motif (Figure 2B). Somewhat surprisingly, anti-Flag IP of MKK7β also pulled-down CaNA-myc (Figure 2B), suggesting that both MKKγ and MKK7β may be present in complexes with CaN in cells. However, anti-Flag IP of the shorter MKK7α isoform lacking the entire N-terminal domain failed to precipitate CaN (Figure 2A, C). Likewise, anti-myc IP of CaNA lead to co-IP of both MKK7β and MKKγ (Figure 2D), but not MKK7α (Figure 2E). Non-immune IgG control IPs also failed to precipitate Flag-MKK7 or CaNA-myc under any of the above conditions, further demonstrating specificity of the interactions of CaNA with MKK7β and MKK7γ.

In order to test whether formation of complexes containing CaN and MKK7β and γ in HEK-293 cells involve CaNA docking to PxIxIT motifs, we overexpressed PVIVIT-GFP as a high-affinity competing PxIxIT binding partner for CaNA (Figure 3A). Accordingly, anti-FLAG co-IP of CaNA-myc with MKK7β or MKKγ (Figure 3B) and anti-myc co-IP of Flag-MKKβ or MKKγ with CaNA-myc (Figure 3C) were all prevented by VIVIT-GFP overexpression (Figure 3D). Thus, co-precipitation of CaNA with MKKγ, as well as MKK7β, requires the PxIxIT motif docking site on CaNA where PVIVIT binds. Next, we began to evaluate the relative affinities of the

Molecular Pharmacology Fast Forward. Published on November 7, 2018 as DOI: 10.1124/mol.118.113159
This article has not been copyedited and formatted. The final version may differ from this version.

PxIxIT site interactions of CaN in complexes with MKKγ and MKK7β by varying the amount of expression of the competing PVIVIT-GFP protein (Figure 4A,B). Consistent with a potentially higher affinity PxIxIT interaction between CaNA and MKKγ compared to MKK7β, higher levels of VIVIT-GFP expression were required to prevent anti-myc CaNA co-IP of Flag-MKK7γ than of Flag-MKK7β (Figure 4B).

However, co-IP of CaN with MKK7 β and/or γ from cell extracts could be mediated either by direct binding to the predicted PxIxIT motifs in these proteins or by indirect interaction through unknown PxIxIT-containing proteins that somehow associate with the MKK7β/γ N-terminal domain. Thus, to assay for direct binding between CaN and the predicted PxIxIT motifs in MKK7 γ and β, we synthesized N-biotinylated 18 amino acid peptides corresponding to residues 35 to 52 containing the MKK7γ PIIVIT and MKK7β PTLQLP sequences, coupled them to streptavidin-agarose beads, and then tested these peptides for co-precipitation of CaNA-myc from HEK-293 cell extracts (Figure 4D, E). As a positive control in this assay we used a biotinylated 14 amino acid peptide encoding the PVIVIT sequence (Aramburu *et al.*, 1999), and as negative control we used a biotinylated 18 amino acid Ht31 peptide, that binds to PKA but not CaN (Carr *et al.*, 1992; Dell'Acqua *et al.*, 2002). While the MKK7γ peptide pulled-down CaNA-myc to a similar extent as the PVIVIT positive control peptide, the MKK7β peptide behaved similar to the Ht31 negative control peptide and failed to precipitate CaNA-myc (Figure 4E). Lastly, we assayed for direct binding of the MKK7γ versus β 35-52 peptides to purified CaN *in vitro* by competition with PVIVIT. In this assay, CaN binding to fluorescently labeled VIVIT peptide was detected by increased fluorescence polarization (anisotropy) due to formation of the larger, slower rotating CaN-peptide complex compared to the free peptide (Figure 4F) (Li *et al.*, 2004). Increasing concentrations of unlabeled MKK7γ, MKK7β, or VIVIT peptides were added to compete with fluorescent-VIVIT binding, causing a decrease in the polarization signal (Figure 4F). In this assay, the MKK7γ peptide competed with an IC_{50}~10 μM,

Molecular Pharmacology Fast Forward. Published on November 7, 2018 as DOI: 10.1124/mol.118.113159
This article has not been copyedited and formatted. The final version may differ from this version.

which was nearly as effective as unlabeled VIVIT peptide competing against itself. In contrast, the MKK7β peptide showed at best partial competition of fluorescent-VIVIT binding and only at much higher doses approaching ~1 mM (Figure 4F). Based on the known K_d of ~0.5 μM for the VIVIT-CaN interaction, we can estimate that the MKK7γ PIIVIT consensus PxIxIT motif binds to CaN with an affinity in the physiologically relevant low-micromolar range. In contrast, the MKK7β PTLQLP non-consensus sequence engages in little or no direct interaction with CaN except at very high concentrations that may be non-physiological (i.e. > 1 mM)

These *in vitro* CaN binding results indicate that MKK7γ engages in a reasonably high-affinity, direct PxIxIT site interaction with CaN that could easily account for the co-IP with CaNA from cell extracts observed above. However, the at best very low affinity interaction detected for the MKK7β peptide with CaN indicates that co-IP of these proteins from cells is likely indirect and must mediated by additional protein interactions in the complex. Thus, we next turned to fluorescence resonance energy transfer (FRET) microscopy to measure possible direct interactions between CaNA and MKK7γ versus MKK7β in living cells. We expressed CaNA C-terminally tagged with CFP and MKK7 α (Figure 5A,G), β (Figure 5B,G), or γ (Figure 5C,F) N-terminally tagged with YFP in COS7 cells. As in our past FRET analysis of the AKAP79-CaNA interaction in living cells (Oliveria et al., 2007; Oliveria et al., 2003), we measured FRET between the CaNA-CFP and YFP-MKK7 by two independent intensity-based FRET methods: 3-filter micro-FRET (3F) to measure sensitized FRET emission from the YFP acceptor (FRETc) and YFP photobleaching (PB) to measure CFP donor dequenching (CFPpost > CFPpre intensity). For cells expressing YFP-MKK7α (Figure 5A) or YFP-MKK7β (Figure 5B) no FRET with CaNA-CFP was detected in corrected images of sensitized FRET (FRETc or FRETc(CFP) gated to the CFP donor channel) and no dequenching of CaNA-CFP fluorescence was seen after YFP PB (CFPpost ~ CFPpre). In contrast, both FRETc signals and YFP PB induced increases in CFPpost > CFPpre fluorescence were observed in the cytoplasm of cells

Molecular Pharmacology Fast Forward. Published on November 7, 2018 as DOI: 10.1124/mol.118.113159
This article has not been copyedited and formatted. The final version may differ from this version.

expressing YFP-MKK7γ and CaNA-CFP (Figure 5C). Quantification from multiple cells of sensitized 3F FRET as apparent FRET efficiency (Eeff) (Figure 5D) (see Materials and Methods) all confirmed significant FRET between YFP-MKK7γ and CaNA-CFP in the cytoplasm and a lack of FRET for MKK7α and MKK7β. In addition, calculation of Eeff from YFP PB measurements of CFP dequenching independently confirmed significant FRET specifically between YFP-MKK7γ and CaNA-CFP (Figure 5E). Thus, these FRET measurements in living cells are in agreement with the *in vitro* binding studies above and provide additional evidence in support of a direct, high-affinity interaction between CaN and MKK7γ, but not MKK7 β or α.

Another notable observation of these imaging experiments was that YFP-MKK7α (Figure 5A) and MKK7β (Figure 5B) were localized in both the nucleus and the cytoplasm, but with greater accumulation in the nucleus. In contrast, YFP-MKK7γ was predominantly found in the cytoplasm with CaNA-CFP where FRET between these two proteins was also detected (Figure 5C). Independent quantification of cytoplasm to nucleus fluorescence intensity ratios confirmed this differential distribution of MKK7 isoforms, with MKK7γ and CaNA exhibiting ratios of >1.0, indicating cytoplasmic enrichment, and MKK7α and MKK7β both showing ratios of <1.0, indicating nuclear enrichment (Figure 5E). Thus, these imaging results indicate that MKK7γ binds directly to CaNA in the cytoplasm, while MKK7α and MKK7β, which do not directly interact with CaNA are more prevalent in the nucleus. Overall, these results reinforce the conclusion that CaN co-IP with MKK7β in Figures 2-4 is due to CaN binding to additional proteins that may associate through the MKK7 N-terminal domain that is absent in MKK7α. In addition, given the observed differences in localization of MKK7β and CaN along with the lack of FRET, the interaction seen in lysates by co-IP may not be relevant in intact cells.

To test the specific role of the MKK7γ consensus PxIxIT motif in mediating localization and FRET with CaN in the cytoplasm, we introduced an in-frame deletion of residues 41PIIVIT46 to create a CFP-MKK7γΔPIX mutant (Figure 6A-B, E-F). As above for YFP-MKKγ

Molecular Pharmacology Fast Forward. Published on November 7, 2018 as DOI: 10.1124/mol.118.113159
This article has not been copyedited and formatted. The final version may differ from this version.

FRET with CaNA-CFP, CFP-MKK7γ and CaNA-YFP exhibited significant cytoplasmic FRETc and CFPpost PB dequenching signals in the cytoplasm of living COS7 cells (Figure 6A). In contrast, the CFP-MKK7γΔPIX mutant failed to show any FRET with CaNA-YFP and was now clearly present in both the nucleus and the cytoplasm (Figure 6B). Quantification of Eeff from sensitized 3F FRET measurements and independently from YFP PB measurements of CFP dequenching for multiple cells both confirmed lack of FRET between CFP-MKK7γΔPIX and CaNA-YFP (Figure 6C). Additional measurements of cytoplasmic/nucleus ratios confirmed significantly reduced localization of MKK7γΔPIX in the cytoplasm compared to MKK7γ wild-type and CaN (Figure 6D). Indeed, the cytoplasmic/nucleus ratio for CFP-MKK7γΔPIX was ~1.0 indicating equal distribution between the cytoplasm and nucleus. Thus, the PIIVIT consensus PxIxIT motif in MKK7γ is required for direct binding to CaNA in the cytoplasm detected as FRET in living cells (Figure 6 E-F) and also prevents MKK7γ from localizing more strongly in the nucleus like the MKK7α and β isoforms, which do not interact directly with CaN.

Next, we used the CaN inhibitor cyclosporin A (CsA) to examine whether the phosphatase activity of CaN is required for cytoplasmic retention of MKK7γ. However, treatment of cells co-expressing YFP-MKK7γ and CaNA-WT-CFP with CsA (Figure 7A) did not alter the cytoplasmic/nucleus localization ratios for either MKK7γ (Figure 7C) or CaNA (Figure 7D) and both proteins remained enriched in the cytoplasm relative to the nucleus similar to control conditions, as indicated by cytoplasm to nucleus ratio values all significantly >1.0. Furthermore, co-expression of a catalytically inactive mutant of CaN (CaNA-H151A-YFP) with CFP-MKK7γ (Figure 7B) did not alter the cytoplasm versus nucleus distributions of MKK7γ or CaNA, and additional treatment with CsA also had no effect (Figure 7C,D). Thus, CaN-MKK7γ binding, rather than dephosphorylation retains MKK7γ in the cytoplasm.

Nonetheless, having demonstrated a preferential association between CaN and MKK7γ relative to MKK7β, we next asked whether CaN may be more effective at regulating the activity

Molecular Pharmacology Fast Forward. Published on November 7, 2018 as DOI: 10.1124/mol.118.113159
This article has not been copyedited and formatted. The final version may differ from this version.

of MKK7γ. MKK7 catalytic activity is governed by the phosphorylation of two residues in its kinase domain: Ser271 and Thr275. As such, an antibody to phospho-MKK7 (Ser271/Thr275) is a useful proxy for its activity level. We therefore expressed CaNA and either YFP-MKK7β1 or YFP-MKK71γ in HEK-293FT cells and treated with vehicle or a CaN inhibitor cocktail (2 μM CsA; 2 μM FK-506) for 30 min. Immunoprecipitation of MKK7 followed by immunoblotting for P-MKK7 revealed a significant increase in P-MKK7γ1 signal in response to CaN inhibition (Figure 8A,B). However, no change in P-MKK7β1 signal was detected. Overall, these findings highlight a role for CaN in the isoform-specific regulation of MKK7 activity that is conferred by the presence of a high-affinity PxIxIT motif in MKK7γ1. Having established isoform-specific regulation of MKK7γ phosphorylation by CaN, we next asked whether CaN interaction with MKK7γ was regulated by intracellular calcium. We treated cells expressing myc-CaNA and YFP-MKK7 γ with ionomycin (1 μM, 3 min) and assessed the amount CaNA associated with MKK7γ by co-IP. Consistent with the known Ca^{2+}-independent nature other CaNA-PxIxIT binding interactions (Li *et al.*, 2011), no significant difference was detected in the amount of CaNA associated with MKK7γ following ionomycin treatment (Figure 8C,D)

JNK signaling regulates important functions in the brain including normal neuronal development and apoptotic neuronal cell death following excitotoxic insults (Davies and Tournier, 2012). Accordingly, inspection the Allen Mouse Brain Atlas (Lein et al., 2007) for *in situ* hybridization data for MKK7 mRNA using a probe that detects all 6 isoforms, revealed that MKK7 mRNA is abundantly expressed in multiple brain regions (Fig. 9A), including the cerebellum, cortex and hippocampus, with particularly high levels in the cerebellum and hippocampus (Fig. 9B). In the hippocampus, MKK7 mRNA expression is seen in cell bodies of pyramidal neurons in the CA1 and CA3 regions and of granule neurons in the dentate gyrus (Fig. 9B, C). To assay for expression of the MKK7γ isoform, we performed quantitative real-time PCR (RT-PCR) with γ-specific primers on RNA isolated from mouse cerebellum, cortex, and

Molecular Pharmacology Fast Forward. Published on November 7, 2018 as DOI: 10.1124/mol.118.113159
This article has not been copyedited and formatted. The final version may differ from this version.

hippocampus and readily detected expression of MKK7γ mRNA at similar relative levels to the house-keeping, control gene GAPDH (Fig. 9D). However, when we performed RT-PCR on RNA prepared from primary cultures of rat hippocampal neurons and cerebellar granule neurons, which also contain glial cells, we detected little or no MKK7γ mRNA expression (Fig. 9D). Closer inspection of *in situ* hybridization images revealed that MKK7 mRNA also appeared to be expressed in vascular structures in brain sections (Fig. 9C). We next performed RT-PCR analysis of RNA from cultured rat micro-vascular endothelial cells (rMVEC) and cultured rat vascular smooth muscle cells (rVSMC), and detected MKK7γ mRNA expression only in rVMSC (Fig. 9D). Thus, the detection of MKK7γ mRNA expression in RNA isolated from brain is likely due to its expression in brain vascular smooth muscle cells.

To explore potential interactions between CaN and MKK7-JNK signaling in vascular smooth muscle cells, we treated cultured rVSMC with Arginine-Vasopressin (AVP), a vasoconstrictive/hypertrophic agonist of Gq-coupled V1a receptors that stimulate Ca^{2+} mobilization, muscle contraction, and smooth muscle-specific gene expression through pathways that can involve both JNK and CaN signaling (Fig. 10A)(Garat *et al.*, 2000; Gonzalez Bosc *et al.*, 2005; Higashita *et al.*, 1997; Hill-Eubanks *et al.*, 2003; Kaplan-Albuquerque *et al.*, 2003b; Nemenoff, 1998). As expected, AVP treatment for 5 min increased P-JNK levels in a dose-dependent manner compared to untreated control cells (Fig. 10B). Importantly, incubation of rVSMC with the CaN phosphatase inhibitor CsA further increased AVP-stimulated P-JNK levels (Fig. 10B), indicating negative regulation of the JNK pathway by CaN. This effect of CsA on JNK signaling in rVSMC was confirmed and quantified by JNK IP kinase assays using recombinant GST-c-jun as a substrate (Fig. 10C). We observed that CsA + AVP led to a significant increase in JNK kinase activity above those produced by AVP alone (Fig. 10C). Overall, these data demonstrate cross-talk between CaN and MKK7-JNK signaling in rVSMC where CaN acts as a negative regulator of the JNK pathway and are consistent with the

Molecular Pharmacology Fast Forward. Published on November 7, 2018 as DOI: 10.1124/mol.118.113159
This article has not been copyedited and formatted. The final version may differ from this version.

physical and functional interaction between MKK7γ and CaN identified above in HEK-293 and COS7 cells.

Molecular Pharmacology Fast Forward. Published on November 7, 2018 as DOI: 10.1124/mol.118.113159
This article has not been copyedited and formatted. The final version may differ from this version.

Discussion

Using a combination of *in silico* bioinformatics, *in vitro* biochemical analysis, and FRET imaging in live cells, we successfully characterized a novel binding interaction between the γ isoform of the kinase MKK7 and the phosphatase CaN. In contrast, we found that the MKK7 α and β isoforms do not directly interact with CaN, although the closely related β isoform may interact indirectly with CaN through other proteins. High affinity binding between CaN and MKK7γ *in vitro* depended on a consensus PxIxIT-type docking motif (41PIIVIT46) that is present only in the γ isoform due to alternative splicing of exon 2 within the N-terminal regulatory domain. Importantly, this consensus PxIxIT motif was required for direct binding between CaN and MKK7γ detected in the cytoplasm of living cells by FRET microcopy and prevented MKK7γ from localizing more prominently in the nucleus like the α and β isoforms. Importantly, we also demonstrated that phosphorylation of MKK7γ, but not of MKK7β, is regulated by CaN phosphatase activity. Finally, we found that MKK7γ was expressed is vascular smooth muscle cells where it may promote negative cross-regulation of JNK signaling by CaN in response to stimulation of GPCR signaling by vasoconstrictive/hypertrophic agonists.

Based on peptide competition binding data, the strong consensus PIIVIT motif in MKK7γ binds CaN nearly as well as PVIVIT and AKAP79 IAIIIT, thus making it one of the highest-affinity known CaN binding partners. In contrast, the PTLQLP motif in MKK7β displays little or no direct CaN binding, thus the observed co-IP of CaN and MKK7β must be stabilized by indirect interactions with other proteins associated through the MKK7 N-terminal domain that is not present in MKK7α. In particular, the MKK7 N-terminal domain contains multiple JNK binding determinants including two LxL sites, 30LNL32 located just N-terminal to and 59LQL61 located just C-terminal to the strong-consensus PIIVIT site in MKK7γ (Tournier *et al.*, 1999). In MKK7β this second LxL site is actually part of the non-consensus 41PTLQLP46 site. Thus, JNK binding to the MKK7β/γ N-terminal domain may link MKK7 and CaN to larger JNK signaling scaffolds

Molecular Pharmacology Fast Forward. Published on November 7, 2018 as DOI: 10.1124/mol.118.113159
This article has not been copyedited and formatted. The final version may differ from this version.

where CaN could interact with upstream MAPKKKs like ASK1, which can bind to the CaNB subunit (Liu *et al.*, 2006), and/or scaffolds like JIP1 (Morrison and Davis, 2003). Alternatively, the close proximity of these JNK binding LxL sites to PIIVIT site in MKK7γ also raises the possibility of competition between CaN and JNK binding to MKK7γ N-terminal domain. For instance, binding of the anti-apoptotic regulatory protein cellular FLICE-inhibitory protein (c-$FLIP_L$) to the MKKβ/γ N-terminus competes with JNK binding (Nakajima *et al.*, 2006). Thus, whether CaN competes with JNK binding and/or engages in interactions with additional binding partners in complexes with MKK7β and/or γ remains to be investigated.

Interestingly, the second LxL JNK binding motif in MKK7γ and β is in the sequence context of LxLP, which is similar to a secondary CaN binding LxVP motif found in CaN substrates such as NFAT, the viral CaN inhibitory protein A238L, and the PKA-RII regulatory subunit (Grigoriu *et al.*, 2013; Li *et al.*, 2011; Martinez-Martinez *et al.*, 2006). LxVP motifs bind CaNA, not at the PxIxIT motif-β sheet binding site in the catalytic domain, but at a site that is overlapping with where CaN-inhibitory immunosuppressant drug-immunophilin complexes (i.e. CsA-cyclophilin) bind in the hinge between the CaNA catalytic domain and C-terminal regulatory domain where CaNB binds (Grigoriu *et al.*, 2013; Rodriguez *et al.*, 2009). Thus, MKK7γ could potentially use both a consensus PxIxIT motif and an LxVP-related motif to interact with CaNA, while MKK7β could potentially very weakly bind to CaN either using PTLQLP as a variant of a PxIxIT motif or LQLP as a variant of the LxVP motif. Consistent with this possibility, CaN was recently shown to bind to an LxL JNK binding motif in the downstream JNK target c-Jun (Goldman *et al.*, 2014). Such an interaction of the MKK7β LQLP motif at the CaN LxVP binding site could also explain the sensitivity of the MKK7β-CaN interaction to competition by PVIVIT, despite a lack of FRET in cells or of high-affinity direct binding *in vitro*, as it is known that at high concentrations PxIxIT motif peptides can cross-bind to the LxVP site (Martinez-Martinez *et al.*, 2006). However, while we found that retention of MKK7γ in the cytoplasm by CaN required its

Molecular Pharmacology Fast Forward. Published on November 7, 2018 as DOI: 10.1124/mol.118.113159
This article has not been copyedited and formatted. The final version may differ from this version.

binding to the PxIxIT motif, inhibition of CaN substrate binding at the LxVP binding site with the immunosuppressant CsA did not alter MKK7γ localization. Thus, while our results cannot completely rule out secondary CaNA binding to an LxVP-like motif in MKK7γ or β, they indicate that this site is not essential for interaction between MKK7γ and CaN.

Our data support a model in which CaN binding to MKK7γ in the cytoplasm allows CaN to regulate MKK7-JNK signaling preferentially in this compartment, as opposed to the nucleus where MKK7 α and β may play more important roles. While the catalytic activity of CaN was not required for maintaining CaNA and MKK7γ in the cytoplasm, CaN was capable of regulating MKK7γ activity through dephosphorylation of the Ser and Thr residues in the MKK7 activation loop. Alternatively, CaN scaffolding to MKK7γ may also position it for dephosphorylation of upstream MAPKKKs on Ser/Thr or downstream JNKs on Thr in their activation loops. Interestingly, MKK7 is a more specific regulator of JNK than MKK4, which also has some weak activity toward p38. In addition, MKK7 preferentially phosphorylates JNK on Thr in the activation loop compared to MKK4, which phosphorylates Thr and Tyr more equally (Wang *et al.*, 2007). Importantly, JNKs are unique within the MAP kinase super-family in that they can be substantially regulated by Thr phosphorylation alone. Thus, dephosphorylation of either MKK7 Ser/Thr phosphorylation or JNK Thr phosphorylation by CaN anchored to MKK7γ would be effective in inhibiting JNK pathway activity as we observed in rVSMC. However, future studies will need to be undertaken to specifically address the role for CaN anchoring to MKK7γ and its PxIxIT motif in these different possible mechanisms of JNK regulation in rVSMC. Future studies will also need to be undertaken to specifically address whether crosstalk between CaN and MKK7-JNK is signaling is preferentially directed to the cytoplasm where the CaN-MKK7γ complex is found in addition to previously described crosstalk in the nucleus where CaN binds to c-Jun (Goldman *et al.*, 2014).

Regardless of the detailed mechanisms, such crosstalk between CaN and JNK could be very important for regulation of vascular remodeling during injury and progression of atherosclerosis where there is important balanced regulation of VSMC differentiation by growth factors, like PDGF, and vasoconstrictive agonists, like AVP, between contractile/smooth muscle and motile/proliferative fibroblast-like phenotypes (Kaplan-Albuquerque *et al.*, 2003a; Kaplan-Albuquerque *et al.*, 2003b; Nemenoff, 1998). Importantly, vasoconstrictive agonists, like AVP and UTP, activate smooth-muscle-specific gene expression programs associated with the contractile phenotype through both JNK regulation of the transcription factor Serum Response Factor (SRF) and CaN activation of NFAT (Garat *et al.*, 2000; Gonzalez Bosc *et al.*, 2005; Hill-Eubanks *et al.*, 2003; Nemenoff, 1998). Thus, CaN binding to MKK7γ in the cytoplasm could negatively regulate JNK signaling to SRF in the nucleus both by promoting MKK7 retention in the cytoplasm and by inhibiting JNK activation/phosphorylation. However, JNK itself can act as a negative regulator of CaN-NFAT signaling in vascular smooth muscle by phosphorylating NFAT4/c3 in the nucleus to promote export (Gomez *et al.*, 2003). Thus, CaN negative regulation of MKK7-JNK signaling may also have positive effects on CaN-NFAT activation in VSMC. Needless to stay, numerous exciting possibilities for cross-regulation of CaN and MKK7-JNK signaling in VSMC remain to be explored that could be important for understanding mechanisms of vascular injury/repair both normally and during vascular disease states.

Molecular Pharmacology Fast Forward. Published on November 7, 2018 as DOI: 10.1124/mol.118.113159
This article has not been copyedited and formatted. The final version may differ from this version.

Authorship Contributions:

Participated in research design: Gibson, Woolfrey, Li, Hogan, Heasley, Nemenoff, Dell'Acqua

Conducted experiments: Gibson, Woolfrey, Li, Heasley

Performed data analysis: Gibson, Woolfrey, Li, Hogan, Heasley, Dell'Acqua

Wrote or contributed to the writing of the manuscript: Gibson, Woolfrey, Li, Hogan, Heasley, Nemenoff, Dell'Acqua

Molecular Pharmacology Fast Forward. Published on November 7, 2018 as DOI: 10.1124/mol.118.113159
This article has not been copyedited and formatted. The final version may differ from this version.

References

Aramburu J, Garcia-Cozar F, Raghavan A, Okamura H, Rao A and Hogan PG (1998) Selective inhibition of NFAT activation by a peptide spanning the calcineurin targeting site of NFAT. *Mol Cell* **1**(5):627-637.

Aramburu J, Yaffe MB, Lopez-Rodriguez C, Cantley LC, Hogan PG and Rao A (1999) Affinity-driven peptide selection of an NFAT inhibitor more selective than cyclosporin A. *Science* **285**(5436):2129-2133.

Carr DW, Hausken ZE, Fraser ID, Stofko-Hahn RE and Scott JD (1992) Association of the type II cAMP-dependent protein kinase with a human thyroid RII-anchoring protein. Cloning and characterization of the RII-binding domain. *J Biol Chem* **267**(19):13376-13382.

Davies C and Tournier C (2012) Exploring the function of the JNK (c-Jun N-terminal kinase) signalling pathway in physiological and pathological processes to design novel therapeutic strategies. *Biochem Soc Trans* **40**(1):85-89.

Dell'Acqua ML, Dodge KL, Tavalin SJ and Scott JD (2002) Mapping the protein phosphatase-2B anchoring site on AKAP79. Binding and inhibition of phosphatase activity are mediated by residues 315-360. *J Biol Chem* **277**(50):48796-48802.

Erickson MG, Liang H, Mori MX and Yue DT (2003) FRET two-hybrid mapping reveals function and location of L-type Ca2+ channel CaM preassociation. *Neuron* **39**(1):97-107.

Garat C, Van Putten V, Refaat ZA, Dessev C, Han SY and Nemenoff RA (2000) Induction of smooth muscle alpha-actin in vascular smooth muscle cells by arginine vasopressin is mediated by c-Jun amino-terminal kinases and p38 mitogen-activated protein kinase. *J Biol Chem* **275**(29):22537-22543.

Goldman A, Roy J, Bodenmiller B, Wanka S, Landry CR, Aebersold R and Cyert MS (2014) The calcineurin signaling network evolves via conserved kinase-phosphatase modules that transcend substrate identity. *Mol Cell* **55**(3):422-435.

Gomez MF, Bosc LV, Stevenson AS, Wilkerson MK, Hill-Eubanks DC and Nelson MT (2003) Constitutively elevated nuclear export activity opposes Ca2+-dependent NFATc3 nuclear accumulation in vascular smooth muscle: role of JNK2 and Crm-1. *J Biol Chem* **278**(47):46847-46853.

Gonzalez Bosc LV, Layne JJ, Nelson MT and Hill-Eubanks DC (2005) Nuclear factor of activated T cells and serum response factor cooperatively regulate the activity of an alpha-actin intronic enhancer. *J Biol Chem* **280**(28):26113-26120.

Gorski JA, Gomez LL, Scott JD and Dell'Acqua ML (2005) Association of an A-kinase-anchoring protein signaling scaffold with cadherin adhesion molecules in neurons and epithelial cells. *Mol Biol Cell* **16**(8):3574-3590.

Grigoriu S, Bond R, Cossio P, Chen JA, Ly N, Hummer G, Page R, Cyert MS and Peti W (2013) The molecular mechanism of substrate engagement and immunosuppressant inhibition of calcineurin. *PLoS Biol* **11**(2):e1001492.

Higashita R, Li L, Van Putten V, Yamamura Y, Zarinetchi F, Heasley L and Nemenoff RA (1997) Galpha16 mimics vasoconstrictor action to induce smooth muscle alpha-actin in vascular smooth muscle cells through a Jun-NH2-terminal kinase-dependent pathway. *J Biol Chem* **272**(41):25845-25850.

Hill-Eubanks DC, Gomez MF, Stevenson AS and Nelson MT (2003) NFAT regulation in smooth muscle. *Trends Cardiovasc Med* **13**(2):56-62.

Kaplan-Albuquerque N, Garat C, Desseva C, Jones PL and Nemenoff RA (2003a) Platelet-derived growth factor-BB-mediated activation of Akt suppresses smooth muscle-specific gene expression through inhibition of mitogen-activated protein kinase and redistribution of serum response factor. *J Biol Chem* **278**(41):39830-39838.

Kaplan-Albuquerque N, Garat C, Van Putten V and Nemenoff RA (2003b) Regulation of SM22 alpha expression by arginine vasopressin and PDGF-BB in vascular smooth muscle cells. *Am J Physiol Heart Circ Physiol* **285**(4):H1444-1452.

Lein ES, Hawrylycz MJ, Ao N, Ayres M, Bensinger A, Bernard A, Boe AF, Boguski MS, Brockway KS, Byrnes EJ, Chen L, Chen TM, Chin MC, Chong J, Crook BE, Czaplinska A, Dang CN, Datta S, Dee NR, Desaki AL, Desta T, Diep E, Dolbeare TA, Donelan MJ, Dong HW, Dougherty JG, Duncan BJ, Ebbert AJ, Eichele G, Estin LK, Faber C, Facer BA, Fields R, Fischer SR, Fliss TP, Frensley C, Gates SN, Glattfelder KJ, Halverson KR, Hart MR, Hohmann JG, Howell MP, Jeung DP, Johnson RA, Karr PT, Kawal R, Kidney JM, Knapik RH, Kuan CL, Lake JH, Laramee AR, Larsen KD, Lau C, Lemon TA, Liang AJ, Liu Y, Luong LT, Michaels J, Morgan JJ, Morgan RJ, Mortrud MT, Mosqueda NF, Ng LL, Ng R, Orta GJ, Overly CC, Pak TH, Parry SE, Pathak SD, Pearson OC, Puchalski RB, Riley ZL, Rockett HR, Rowland SA, Royall JJ, Ruiz MJ, Sarno NR, Schaffnit K, Shapovalova NV, Sivisay T, Slaughterbeck CR, Smith SC, Smith KA, Smith BI, Sodt AJ, Stewart NN, Stumpf KR, Sunkin SM, Sutram M, Tam A, Teemer CD, Thaller C, Thompson CL, Varnam LR, Visel A, Whitlock RM, Wohnoutka PE, Wolkey CK, Wong VY, Wood M, Yaylaoglu MB, Young RC, Youngstrom BL, Yuan XF, Zhang B, Zwingman TA and Jones AR (2007) Genome-wide atlas of gene expression in the adult mouse brain. *Nature* **445**(7124):168-176.

Li H, Pink MD, Murphy JG, Stein A, Dell'acqua ML and Hogan PG (2012) Balanced interactions of calcineurin with AKAP79 regulate Ca(2+)-calcineurin-NFAT signaling. *Nat Struct Mol Biol* **19**(3):337-345.

Li H, Rao A and Hogan PG (2004) Structural delineation of the calcineurin-NFAT interaction and its parallels to PP1 targeting interactions. *J Mol Biol* **342**(5):1659-1674.

Li H, Rao A and Hogan PG (2011) Interaction of calcineurin with substrates and targeting proteins. *Trends Cell Biol* **21**(2):91-103.

Li H, Zhang L, Rao A, Harrison SC and Hogan PG (2007) Structure of calcineurin in complex with PVIVIT peptide: portrait of a low-affinity signalling interaction. *J Mol Biol* **369**(5):1296-1306.

Liu Q, Wilkins BJ, Lee YJ, Ichijo H and Molkentin JD (2006) Direct interaction and reciprocal regulation between ASK1 and calcineurin-NFAT control cardiomyocyte death and growth. *Mol Cell Biol* **26**(10):3785-3797.

Martinez-Martinez S, Rodriguez A, Lopez-Maderuelo MD, Ortega-Perez I, Vazquez J and Redondo JM (2006) Blockade of NFAT activation by the second calcineurin binding site. *J Biol Chem* **281**(10):6227-6235.

Morrison DK and Davis RJ (2003) Regulation of MAP kinase signaling modules by scaffold proteins in mammals. *Annu Rev Cell Dev Biol* **19**:91-118.

Murphy JG, Sanderson JL, Gorski JA, Scott JD, Catterall WA, Sather WA and Dell'Acqua ML (2014) AKAP-anchored PKA maintains neuronal L-type calcium channel activity and NFAT transcriptional signaling. *Cell Rep* **7**(5):1577-1588.

Nakajima A, Komazawa-Sakon S, Takekawa M, Sasazuki T, Yeh WC, Yagita H, Okumura K and Nakano H (2006) An antiapoptotic protein, c-FLIPL, directly binds to MKK7 and inhibits the JNK pathway. *EMBO J* **25**(23):5549-5559.

Nemenoff RA (1998) Vasopressin signaling pathways in vascular smooth muscle. *Front Biosci* **3**:d194-207.

Oliveria SF, Dell'Acqua ML and Sather WA (2007) AKAP79/150 anchoring of calcineurin controls neuronal L-type Ca2+ channel activity and nuclear signaling. *Neuron* **55**(2):261-275.

Oliveria SF, Dittmer PJ, Youn DH, Dell'acqua ML and Sather WA (2012) Localized calcineurin confers Ca2+-dependent inactivation on neuronal L-type Ca2+ channels. *J Neurosci* **32**(44):15328-15337.

Oliveria SF, Gomez LL and Dell'Acqua ML (2003) Imaging kinase--AKAP79--phosphatase scaffold complexes at the plasma membrane in living cells using FRET microscopy. *J Cell Biol* **160**(1):101-112.

Rodriguez A, Roy J, Martinez-Martinez S, Lopez-Maderuelo MD, Nino-Moreno P, Orti L, Pantoja-Uceda D, Pineda-Lucena A, Cyert MS and Redondo JM (2009) A conserved docking surface on calcineurin mediates interaction with substrates and immunosuppressants. *Mol Cell* **33**(5):616-626.

Sanderson JL, Gorski JA, Gibson ES, Lam P, Freund RK, Chick WS and Dell'Acqua ML (2012) AKAP150-anchored calcineurin regulates synaptic plasticity by limiting synaptic incorporation of Ca2+-permeable AMPA receptors. *J Neurosci* **32**(43):15036-15052.

Schnell U, Dijk F, Sjollema KA and Giepmans BN (2012) Immunolabeling artifacts and the need for live-cell imaging. *Nat Methods* **9**(2):152-158.

Sorkin A, McClure M, Huang F and Carter R (2000) Interaction of EGF receptor and grb2 in living cells visualized by fluorescence resonance energy transfer (FRET) microscopy. *Curr Biol* **10**(21):1395-1398.

Tournier C, Whitmarsh AJ, Cavanagh J, Barrett T and Davis RJ (1999) The MKK7 gene encodes a group of c-Jun NH2-terminal kinase kinases. *Mol Cell Biol* **19**(2):1569-1581.

Wang X, Destrument A and Tournier C (2007) Physiological roles of MKK4 and MKK7: insights from animal models. *Biochim Biophys Acta* **1773**(8):1349-1357.

Wild AR and Dell'Acqua ML (2018) Potential for therapeutic targeting of AKAP signaling complexes in nervous system disorders. *Pharmacol Ther* **185**:99-121.

Woolfrey KM and Dell'Acqua ML (2015) Coordination of Protein Phosphorylation and Dephosphorylation in Synaptic Plasticity. *J Biol Chem* **290**(48):28604-28612.

Woolfrey KM, Sanderson JL and Dell'Acqua ML (2015) The palmitoyl acyltransferase DHHC2 regulates recycling endosome exocytosis and synaptic potentiation through palmitoylation of AKAP79/150. *J Neurosci* **35**(2):442-456.

Footnotes:

*This research was supported by grants from the National Institutes of Health (NIH) to M.L.D [MH102338, NS040701], to Anjana Rao and P.G.H [AI040127], to H.L. [AI090428], to L.E.H. [CA116527] and to R.A.N [CA162226 and CA058187]. Contents are the authors' sole responsibility and do not necessarily represent official NIH views. The authors declare no competing financial interests.

†Reprint requests can be addressed to Mark L. Dell'Acqua, Dept. of Pharmacology, 12800 E. 19th Ave, Mail Stop 8303, Aurora, CO 80045. Email: mark.dellacqua@ucdenver.edu

Molecular Pharmacology Fast Forward. Published on November 7, 2018 as DOI: 10.1124/mol.118.113159
This article has not been copyedited and formatted. The final version may differ from this version.

Figure Legends

Figure 1: MKK7γ contains a putative consensus PxIxIT docking motif for CaN. (**A**) Sequence alignments within the N-terminal domains of MKK7γ and MKK7β showing how alternative splicing of exon 2 introduces 17 amino acids that are unique to MKK7γ and contain a putative consensus PxIxIT motif 41PIIVIT46. An alternate alignment of the MKK7β N-terminal domain sequence reveals a possible non-consensus PxIxIT motif variant of PTLQLP. (**B**) Diagram of the role of MKK7 as a MAPKK (along with MKK4) in the JNK MAPK signaling pathway. (**C**) Diagrams of the three N-terminal (α, β, γ) and two C-terminal (1, 2) alternatively spliced isoforms of MKK7. Locations of the common kinase domain, the JNK binding N-terminal domain, and the potential CaN binding PxIxIT motifs are indicated.

Figure 2: MKK7γ and MKK7β co-immunoprecipitate with CaN from HEK-293 cells. (**A**) Diagram showing the experimental design detecting reciprocal co-IP of CaNA-myc and Flag-MKK7γ and -MKK7β but not -MKK7α from transfected HEK-293 cells. (**B**) Co-IP of CaNA-myc, detected by anti-myc immunoblotting (IB) with anti-Flag pull-down of Flag-MKK7γ1 and Flag-MKK7β1 but not non-immune rabbit IgG. (**C**) No co-IP of CaNA-myc with Flag-MKK7α1. (**D**) Co-IP of Flag-MKK7γ1 and Flag-MKK7β1 detected by anti-Flag IB with anti-myc pull-down of CaNA-myc but not non-immune mouse IgG. (**E**) No co-IP Flag-MKK7α1 with CaNA-myc. All data are representative of 3 independent experiments.

Figure 3: A competing PxIxIT motif PVIVIT prevents CaN co-immunoprecipitation with MKK7γ and MKK7β. (**A**) Diagram showing the experimental design for detecting PVIVIT-GFP disruption of reciprocal co-IP between CaNA-myc and Flag-MKK7γ and -MKK7β in HEK-293 cells. (**B**) Expression of PVIVIT (bottom panel, +VIVIT-GFP) prevents normal anti-Flag co-IP of CaNA-myc with Flag-MKK7γ1 and Flag-MKK7β1 (top panel, -VIVIT-GFP). (**C**) Expression of

Molecular Pharmacology Fast Forward. Published on November 7, 2018 as DOI: 10.1124/mol.118.113159
This article has not been copyedited and formatted. The final version may differ from this version.

PVIVIT (bottom panel, +VIVIT-GFP) prevents normal anti-myc co-IP of Flag-MKK7γ1 and Flag-MKK7β1 with CaNA-myc (top panel, -VIVIT-GFP). (**D**) Anti-GFP IB detecting PVIVIT-GFP expression in the extracts used for the anti-Flag and anti-myc IP in panels B and C. All data are representative of 3 independent experiments.

Figure 4: MKK7γ, but not MKK7β, binds to CaN through a direct PxIxIT motif interaction. (**A**) Diagram showing the experimental design for detecting PVIVIT-GFP disruption of anti-myc co-IP of CaNA-myc and Flag-MKK7γ and -MKK7β in HEK-293 cells. (**B**) Transfection of HEK-293 cells with higher amounts of plasmid DNA leading to higher levels of VIVIT-GFP expression (middle panel; IB: GFP) are required to disrupt anti-myc co-IP of Flag-MKK7γ1 and Flag-MKK7β1 (top panel; IB: Flag) with CaNA-myc (bottom panel; IB: myc) (**D**) Diagram showing the experimental design for detecting precipitation of CaNA-myc by biotinylated MKK7β or MKK7γ 35-52 peptides coupled to streptavidin agarose beads. (**E**) MKK7γ 35-52 and PVIVIT biotinylated peptides precipitate CaNA-myc from HEK-293 cell extracts. MKK7β 35-52 and negative control (Ht31) biotinylated peptides do not precipitate CaNA-myc. (**F**) The MKK7γ 35-52 peptide competes with an affinity similar to PVIVIT for fluorescent-PVIVIT binding to CaN measured by fluorescence polarization (mP). MKK7β 35-52 only competes for fluorescent PVIVIT binding to CaN at much higher concentrations. All data are representative of 3 independent experiments.

Figure 5: Interaction between MKK7γ and CaN imaged by FRET microscopy in the cytoplasm of living cells. Sensitized YFP acceptor 3F FRET emission (FRETc) or CFP-donor dequenching following photobleaching (PB) of the YFP-acceptor (CFPpost > CFPpre) is not detected for CaNA-CFP with (**A**) YFP-MKK7α or (**B**) YFP-MKK7β but is detected with (**C**) YFP-MKK7γ in living COS7 cells. The merge panels show overlap (turquoise) of CaNA-CFP (blue)

Molecular Pharmacology Fast Forward. Published on November 7, 2018 as DOI: 10.1124/mol.118.113159
This article has not been copyedited and formatted. The final version may differ from this version.

and YFP-MKK7 (green) localization in the cytoplasm but not the nucleus. FRETc is shown in both monochrome and in pseudocolor on the same relative intensity scales (blue=no FRETc to green, yellow, orange, and red=high with FRETc gated to the CFP donor channel). For YFP PB FRET, CFP donor intensity before (CFPpre) and after (CFPpost) is shown on the same relative pseudocolor intensity scale (blue=no intensity to red=high intensity). Scale bar = 10 μm (**D**) Quantification of sensitized 3F FRET emission and YFP PB CFP dequenching as apparent FRET efficiency (Eeff) for multiple cells showing significant FRET for MKK7γ (Eeff (3F) 0.050±.007, n=12, ***p<0.001 by one-way ANOVA with Bonferonni post-hoc correction for multiple comparisons; Eeff (PB) 0.055±.013, n=8, **p<0.01 by one-way ANOVA with Bonferonni post-hoc correction for multiple comparisons) compared to MKK7α (Eeff (3F) -0.032±.003, n=14; Eeff (PB) -0.022±0.016, n=10) and MKK7β (Eeff (3F) -0.030±0.004, n=14; Eeff (PB) -0.034±0.021, n=12). Eeff values ≤ 0 reflect lack of FRET. (**E**) Quantification of cytoplasm/nucleus fluorescence intensity ratios for multiple cells showing enrichment in the cytoplasm over the nucleus (>1.0) for MKK7γ (1.5±0.1, n=12, 8 ***p<0.001 by one-way ANOVA with Bonferonni post-hoc correction for multiple comparisons) and CaNA (1.63±0.09, n=14, ***p<0.001 by one-way ANOVA with Bonferonni post-hoc correction for multiple comparisons) compared to MKK7α (0.81±0.05, n=14) and MKK7β (0.81±0.05, n=14). (**H**) Diagram depicting CFP-YFP FRET between CaNA-CFP bound to N-terminal domain of YFP-MKK7γ but not (**I**) YFP-MKK7α or YFP-MKK7β. All graphs represent mean ± standard error. Please note that all of the p values above are below a threshold of 0.05/3=0.0167 that incorporates additional correction for multiple-testing due to applying two different CFP-YFP FRET methods and measuring CFP and YFP cytoplasm/nucleus ratios in the same cells.

Molecular Pharmacology Fast Forward. Published on November 7, 2018 as DOI: 10.1124/mol.118.113159
This article has not been copyedited and formatted. The final version may differ from this version.

Figure 6: Deletion of the MKK7γ PxIxIT motif eliminates FRET with CaN and promotes localization to the nucleus. Sensitized YFP acceptor 3F FRET emission (FRETc) or CFP donor dequenching following photobleaching (PB) of the YFP acceptor (CFPpost > CFPpre) is detected for CaNA-YFP with (**A**) CFP-MKK7γ but not (**B**) CFP-MKK7γΔPIX in living COS7 cells. The merge panels show overlap (turquoise) of CaNA-YFP (green) and CFP-MKK7γ (blue) localization in the cytoplasm but not the nucleus. FRETc is shown in both monochrome and in pseudocolor on the same relative intensity scales (blue=no FRETc to green, yellow, orange, and red=high with FRETc gated to the CFP donor channel). For YFP PB FRET, CFP donor intensity before (CFPpre) and after (CFPpost) is shown on the same relative pseudocolor intensity scale (blue=no intensity to red=high intensity). Scale bar = 10 μm (**C**) Quantification of apparent FRET efficiency from sensitized 3F FRET emission (Eeff) and YFP PB CFP dequenching (Eeff (PB)) for multiple cells showing significant FRET for MKK7γ (Eeff (3F)) 0.057±0.007, n=9, ***p<0.001 by unpaired, two-tailed t-test; Eeff (PB) 0.042±0.018, n=9, **p<0.01 by unpaired, two-tailed t-test) compared to MKK7ΔPIXγ (Eeff (3F) -0.056±0.006, n=10; Eeff (PB) -0.004±0.01, n=10). Eeff values ≤ 0 reflect lack of FRET. (**D**) Quantification of cytoplasm/nucleus fluorescence intensity ratios for multiple cells showing enrichment in the cytoplasm (>1.0) for MKK7γ (1.55±0.07, n=9) but equal distribution in the nucleus and cytoplasm (~1.0) for MKK7γΔPIX (1.08±0.09, n=10, ***p=0.0008 by unpaired, two-tailed t-test). (**E**) Diagram depicting CFP-YFP FRET between CaNA-YFP bound to N-terminal domain of CFP-MKK7γ but not (**F**) CFP-MKK7γΔPIX. All graphs represent mean ± standard error. Please note that all of the p values above are below a threshold of 0.05/3=0.0167 that incorporates additional correction for multiple-testing due to applying two different CFP-YFP FRET methods and measuring CFP and YFP cytoplasm/nucleus ratios in the same cells.

Molecular Pharmacology Fast Forward. Published on November 7, 2018 as DOI: 10.1124/mol.118.113159
This article has not been copyedited and formatted. The final version may differ from this version.

Figure 7: CaN phosphatase activity is not required to retain MKK7γ in the cytoplasm. (**A**) Images of fixed COS7 cells expressing YFP-MKK7γ (green) and CaNAWT -CFP (blue) or (**B**) CFP-MKK7γ (blue) and catalytically inactive CaNH151A-YFP (green) under control conditions or after treatment with the CaN phosphatase inhibitor CsA (1 μM) as indicated. The merge panels show overlap (turquoise) of CaNA and MKK7γ localization in the cytoplasm but not the nucleus. Scale bar = 10 μm (**C**) Quantification of cytoplasm/nucleus fluorescence intensity ratios for multiple cells showing maintenance of MKK7γ cytoplasmic enrichment (cytoplasm/nucleus ratios all >1.0 by one-sample t-test: MKK7γ+CaNAWT 1.15±0.03, n=10, **p=0.0014; MKK7γ+CaNAWT+CsA 1.17±0.06, n=10, *p=0.020, MKK7γ+CaNAH151A 1.12±0.03, n=13, **p=0.0024; MKK7γ+CaNAH151A+CsA, 1.09±0.03n=11, **p=0.0094; but all cytoplasm/nucleus ratios not different for any pairwise comparisons p>0.05 n.s. by one-way ANOVA with Bonferonni post-hoc correction for multiple comparisons) and (**D**) CaNA cytoplasmic enrichment (cytoplasm/nucleus ratios >1.0 by one-sample t-test; CaNAWT 1.44±0.06, n=10, ****p<0.0001; CaNAWT+CsA 1.46±0.08, n=10, ***p=0.0003; CaNAH151A 1.52±0.07, n=13, ****p<0.0001; CaNAH151A 1.45±0.05, n=11, ****p<0.0001; but all cytoplasm/nucleus ratios are not different for any pairwise comparisons p>0.05 n.s. by one-way ANOVA with Bonferonni post-hoc correction for multiple comparisons for all conditions). Note: These cytoplasm/nucleus ratios in fixed COS7 cells for both MKK7γ and CaNA are somewhat lower than in live cells (Figure 5G and 6F) likely due to some loss of cytoplasmic FP fluorescence that occurs after fixation (Schnell *et al.*, 2012).

Figure 8. CaN selectively regulates MKK7γ phosphorylation state. (**A**) YFP-MKK7γ1 or β1 was immunoprecipitated (IP) from HEK-293FT cell lysates and samples were immunoblotted (IB) with anti-P-MKK7 to detect phosphorylation at residues Ser271 and Thr275 or anti-GFP to detect total YFP-MKK7 expression. Co-expression of myc-CaN with YFP-MKK7 was confirmed

Molecular Pharmacology Fast Forward. Published on November 7, 2018 as DOI: 10.1124/mol.118.113159
This article has not been copyedited and formatted. The final version may differ from this version.

by immunoblotting of the input cell lysates. (**B**) Quantification of 4 independent experiments such as in panel A showing fold-change change with CaN inhibition for P-MKK7 normalized to total YFP-MKK7 expression. Inhibition of CaN by CsA and FK-506 significantly increased phosphorylation of MKK7γ1 but not of MKK7β1 compared to untreated control conditions (fold-change normalized to untreated controls MKK7γ1 1.4±0.10; MKK7β1, 1.0±0.1, n=4; *p<0.05 for MKK7γ1 but p>0.05 n.s. for MKK7β1 to 1.0 by one-sample t-test). **C**) Co-IP of myc-CaNA with YFP-MKK7γ1 following treatment with ionomycin or vehicle. (**D**) Quantification of co-IP of CaNA with MKK7γ1 revealed no significant impact of elevating intracellular calcium with ionomycin (0.86 +/- 0.05, n = 3 independent experiments, one sample t-test, p>0.05). Please note, though not significant, the trend toward reduced interaction between CaNA and MKK7γ is likely related to a non-significant trend toward reduced total input levels of myc-CaNA (0.67 +/- 0.11, p>0.05) in response to ionomycin in these same experiments.

Figure 9: MKK7γ mRNA is expressed in the brain and cultured vascular smooth muscle cells but not in cultured neurons. (**A**) *In situ* hybridization detecting expression of mRNA for all isoforms of MKK7 in a sagittal section of mouse brain. The cortex (Ctx), cerebellum (Cb) and hippocampus (Hp) are labeled. (**B, C**) Enlargements of the hippocampal region from panel A showing expression of MKK7 mRNA in neuronal cell bodies of the CA1, CA3, and DG regions. Putative vascular structures (Vasc) expressing MKK7 mRNA in the hippocampus are labeled in panel C. MKK7 mRNA *in situ* hybridization images in panels A-C downloaded from the Allen Mouse Brain Atlas [Internet]. Seattle (WA): Allen Institute for Brain Science. ©2009. Available open-access from: http://mouse.brain-map.org. (**D**) Real-time PCR to quantitate MKK7γ mRNA expression relative to GAPDH mRNA expression in mouse (m) cerebellum, cortex, and hippocampus and in rat cultured hippocampal neurons (rHN), cerebellar granule neurons (rCGN), microvascular endothelial cells (rMVEC), and vascular smooth muscle cells (rVSMC).

Molecular Pharmacology Fast Forward. Published on November 7, 2018 as DOI: 10.1124/mol.118.113159
This article has not been copyedited and formatted. The final version may differ from this version.

Figure 10: CaN phosphatase activity inhibits JNK signaling in rat vascular smooth muscle cells. (**A**) Diagram of potential negative regulation of MKK7-JNK signaling downstream of GPCR activation by AVP. (**B**) Incubation with CsA (0.8 μM) increases JNK1/2 phosphorylation (P-JNK1/2) in rVSMC in response to increasing doses of AVP (0.01-1 μM, 5 min) as indicated. Phospho-JNK was detected by immunoblotting with an antibody recognizing the dual-Thr/Tyr phosphorylated JNK1/2 activation loop. (**C**) CsA (0.8 μM) increases (0.1 μM) AVP-stimulated JNK kinase activity (normalized to untreated control cells). JNK activity was measured in cell extracts of rVSMC using an *in vitro* IP-kinase assay that monitors ^{32}P transfer to recombinant GST-c-jun (in cpm) from [γ-^{32}P]-ATP. (Fold-change normalized to untreated controls: AVP 1.53±0.10; AVP+CsA 2.04±0.15, n=3; **p=0.0075 by paired t-test, which is below the Bonferonni corrected p value threshold of 0.05/2=0.025 for multiple comparisons; #p<0.05 by one-sample t-test to 1.0 indicates significant AVP stimulation of JNK activity above respective untreated control conditions for both AVP alone and AVP+CsA).

Molecular Pharmacology Fast Forward. Published on November 7, 2018 as DOI: 10.1124/mol.118.113159
This article has not been copyedited and formatted. The final version may differ from this version.

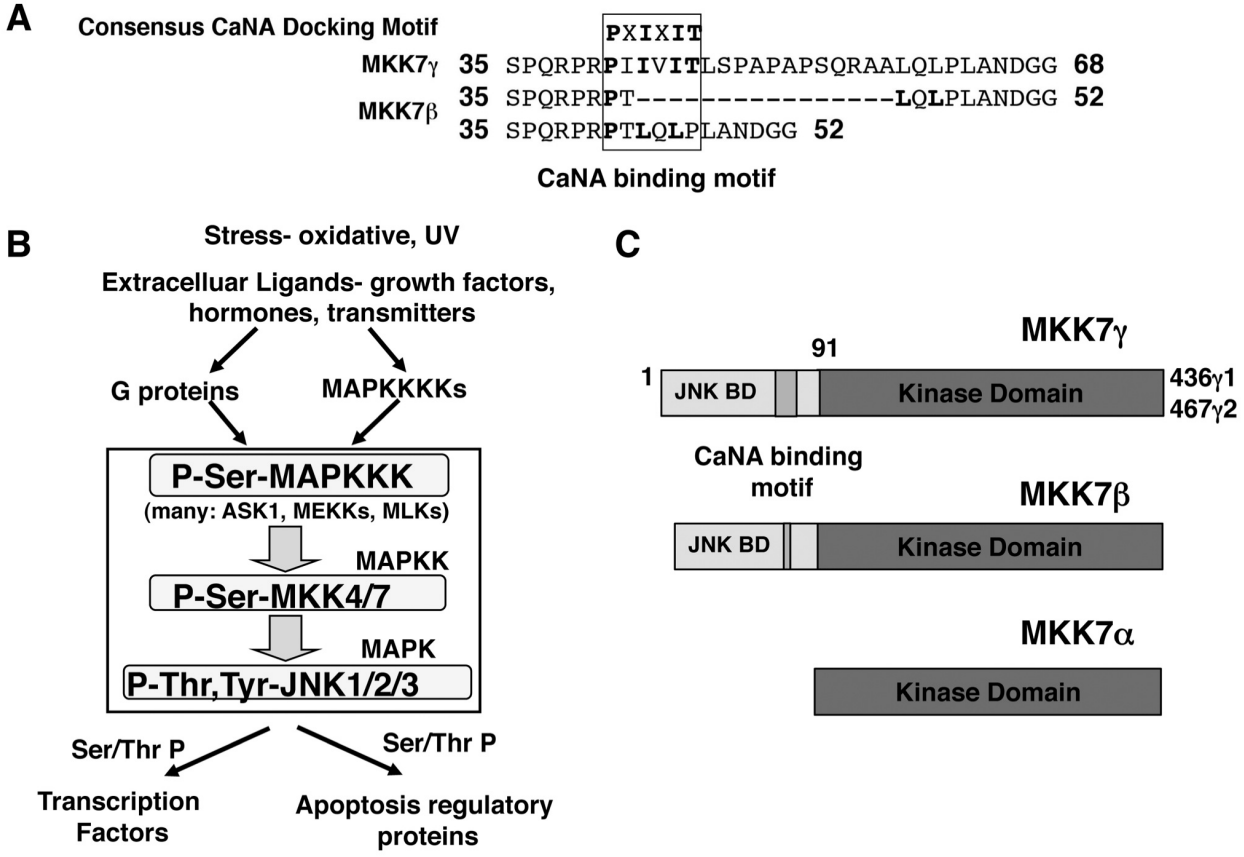

Figure 1

Molecular Pharmacology Fast Forward. Published on November 7, 2018 as DOI: 10.1124/mol.118.113159
This article has not been copyedited and formatted. The final version may differ from this version.

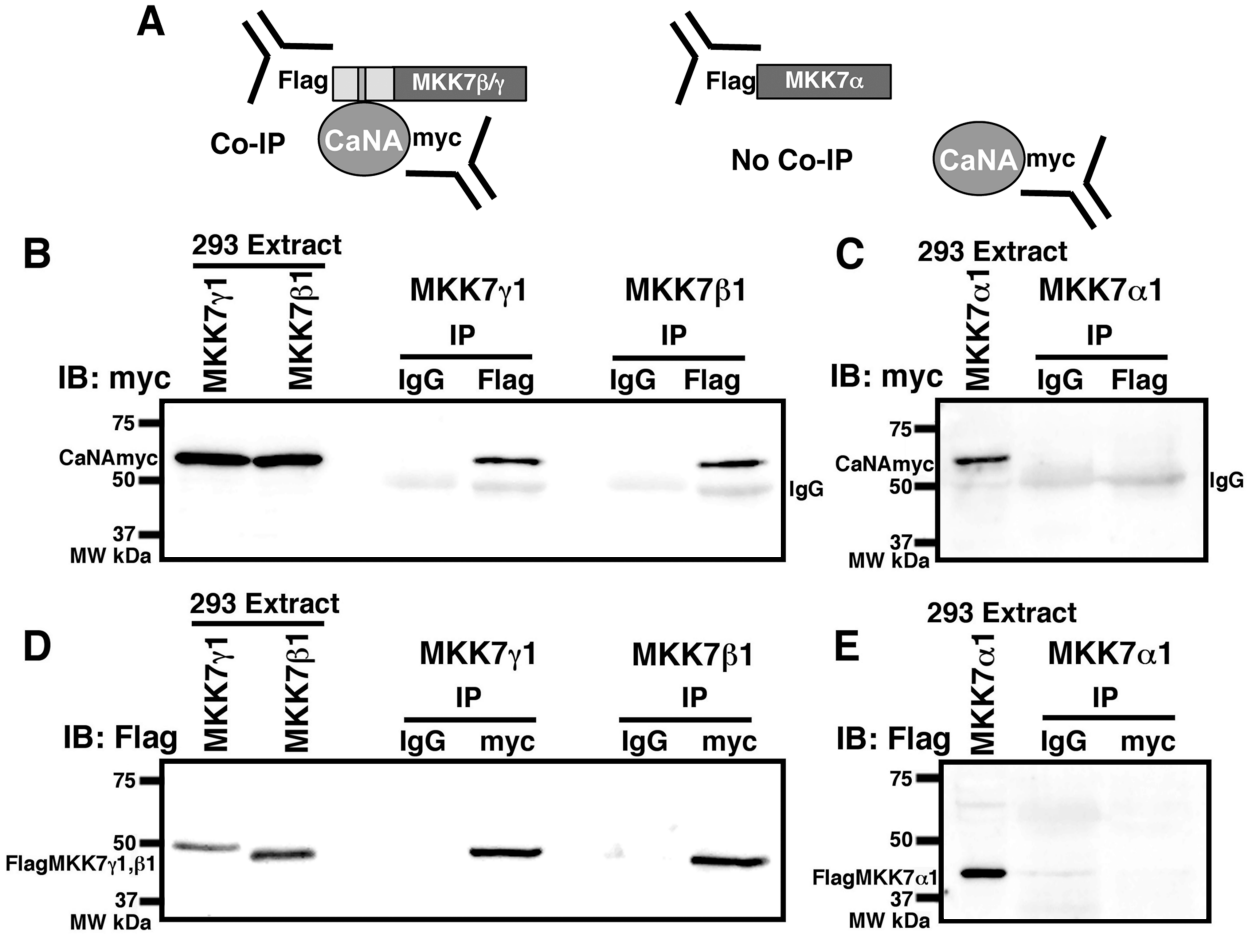

Figure 2

Molecular Pharmacology Fast Forward. Published on November 7, 2018 as DOI: 10.1124/mol.118.113159
This article has not been copyedited and formatted. The final version may differ from this version.

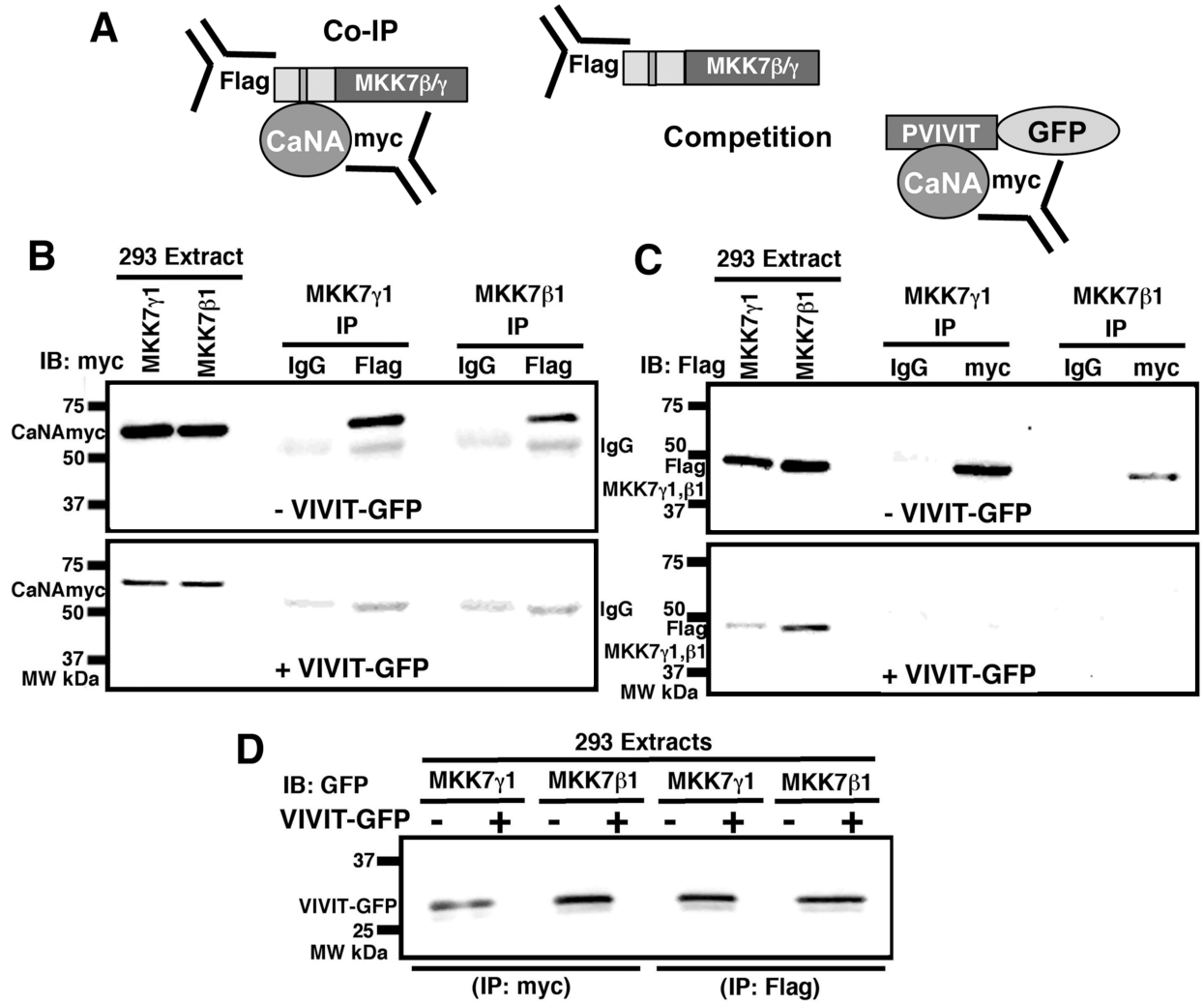

Figure 3

Molecular Pharmacology Fast Forward. Published on November 7, 2018 as DOI: 10.1124/mol.118.113159
This article has not been copyedited and formatted. The final version may differ from this version.

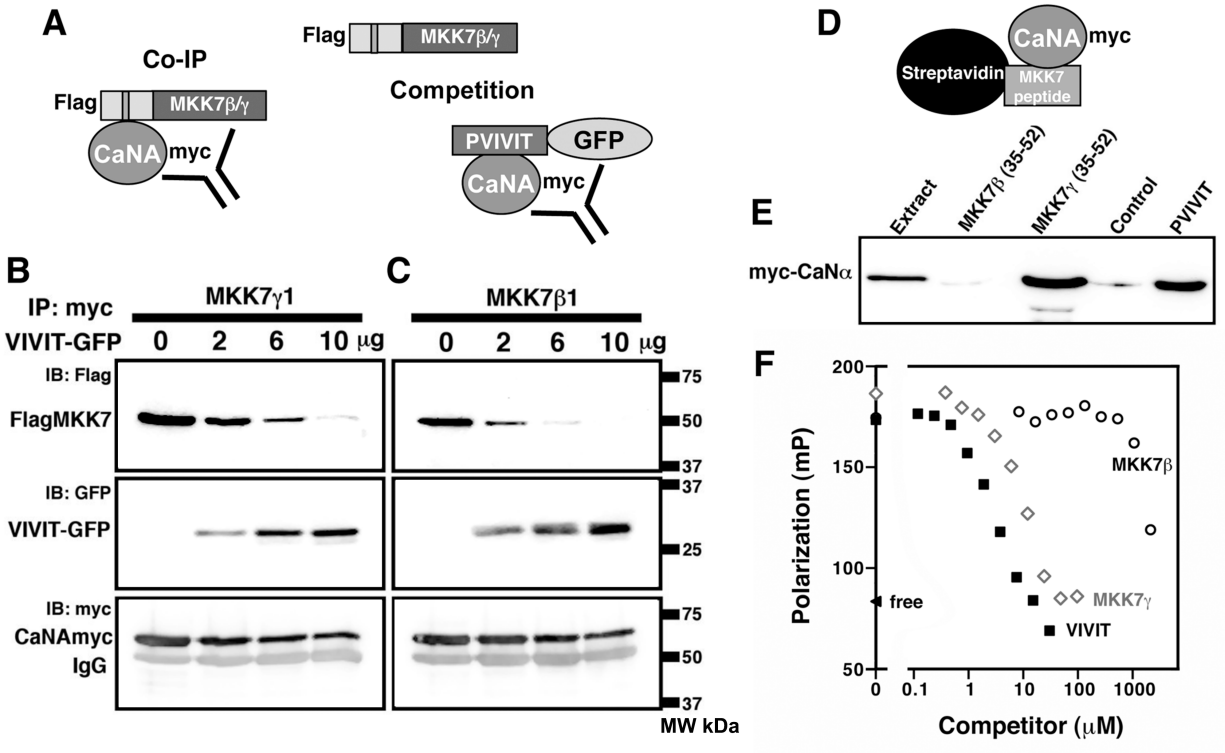

Figure 4

Molecular Pharmacology Fast Forward. Published on November 7, 2018 as DOI: 10.1124/mol.118.113159
This article has not been copyedited and formatted. The final version may differ from this version.

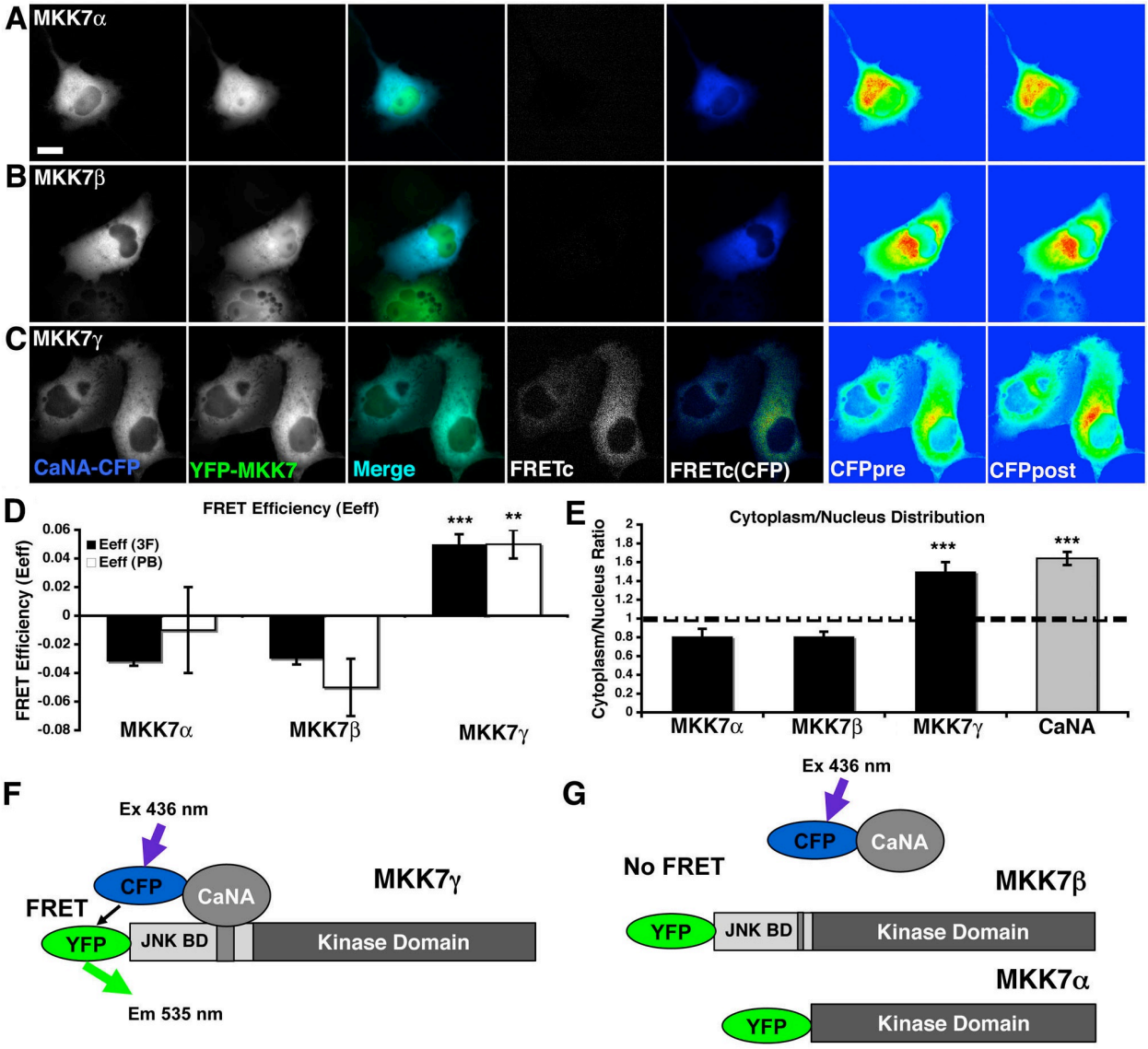

Figure 5

Molecular Pharmacology Fast Forward. Published on November 7, 2018 as DOI: 10.1124/mol.118.113159
This article has not been copyedited and formatted. The final version may differ from this version.

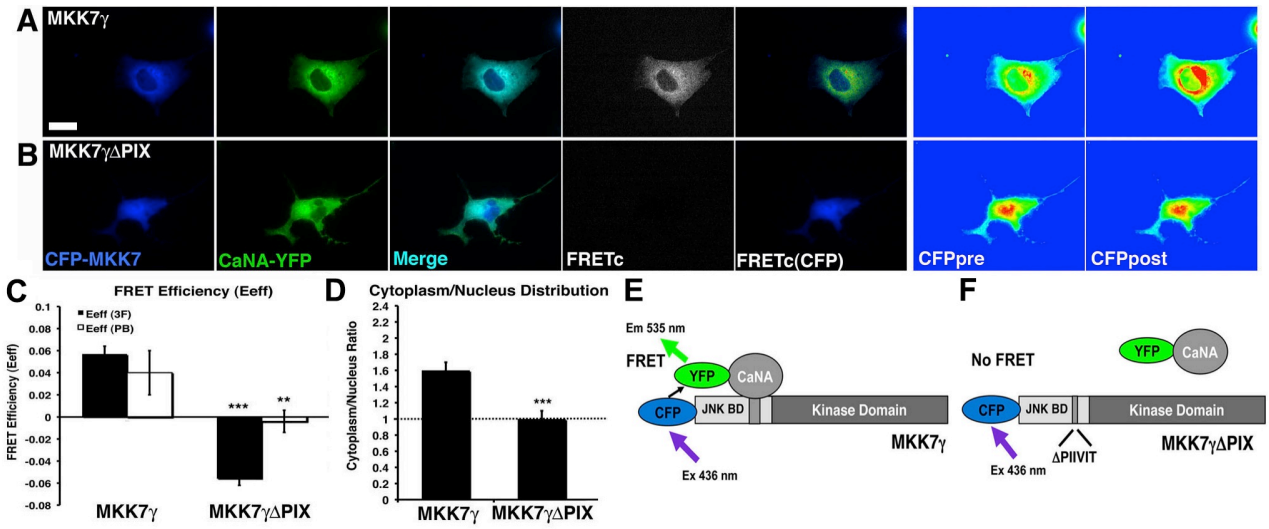

Figure 6

Molecular Pharmacology Fast Forward. Published on November 7, 2018 as DOI: 10.1124/mol.118.113159
This article has not been copyedited and formatted. The final version may differ from this version.

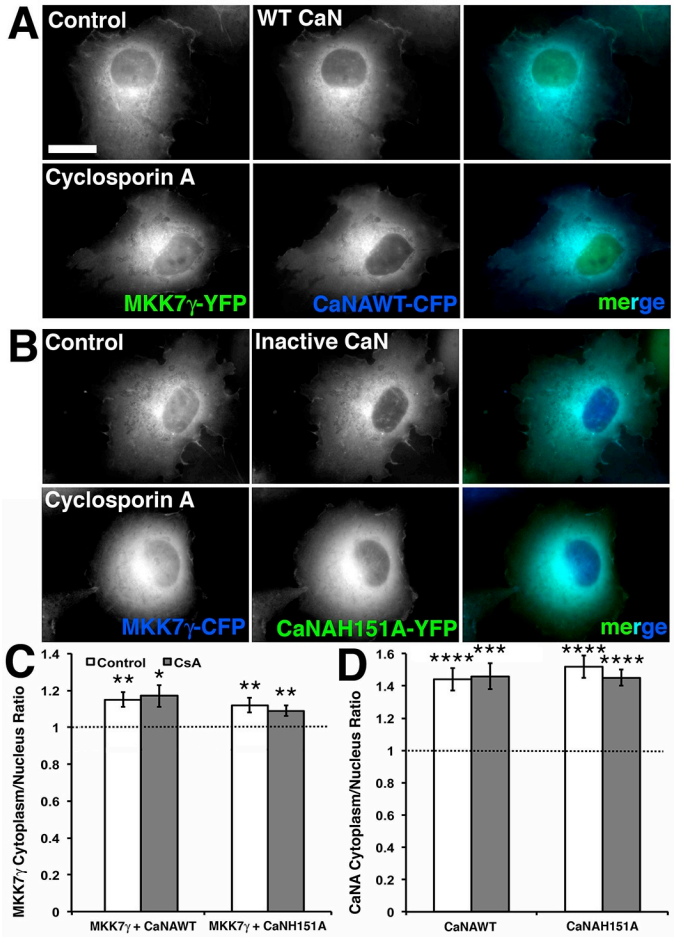

Figure 7

Molecular Pharmacology Fast Forward. Published on November 7, 2018 as DOI: 10.1124/mol.118.113159
This article has not been copyedited and formatted. The final version may differ from this version.

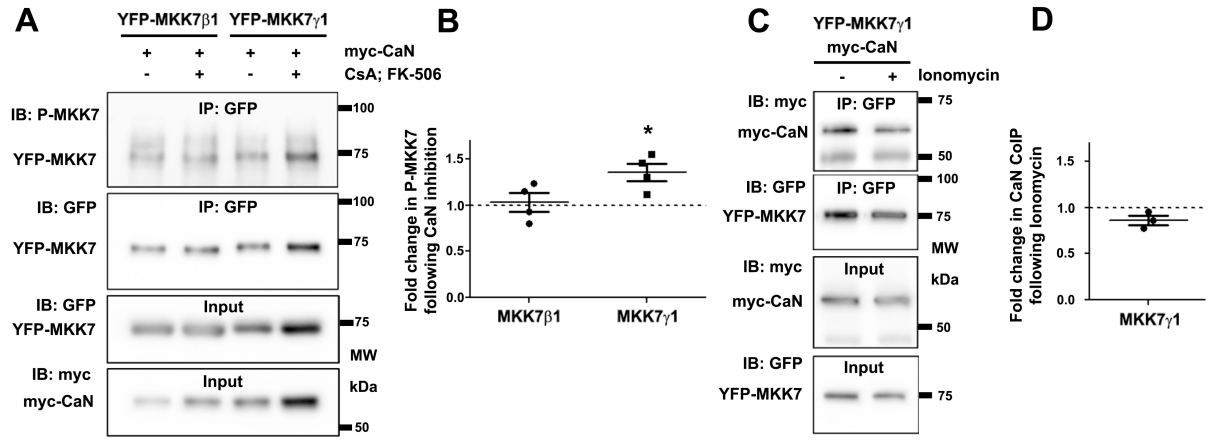

Figure 8

Molecular Pharmacology Fast Forward. Published on November 7, 2018 as DOI: 10.1124/mol.118.113159
This article has not been copyedited and formatted. The final version may differ from this version.

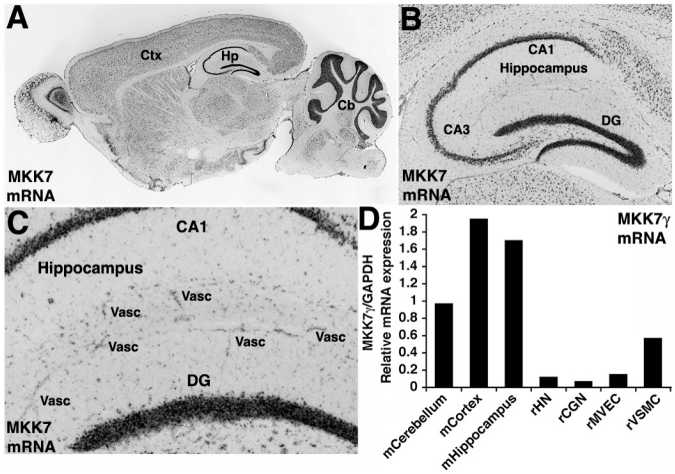

Figure 9

Molecular Pharmacology Fast Forward. Published on November 7, 2018 as DOI: 10.1124/mol.118.113159
This article has not been copyedited and formatted. The final version may differ from this version.

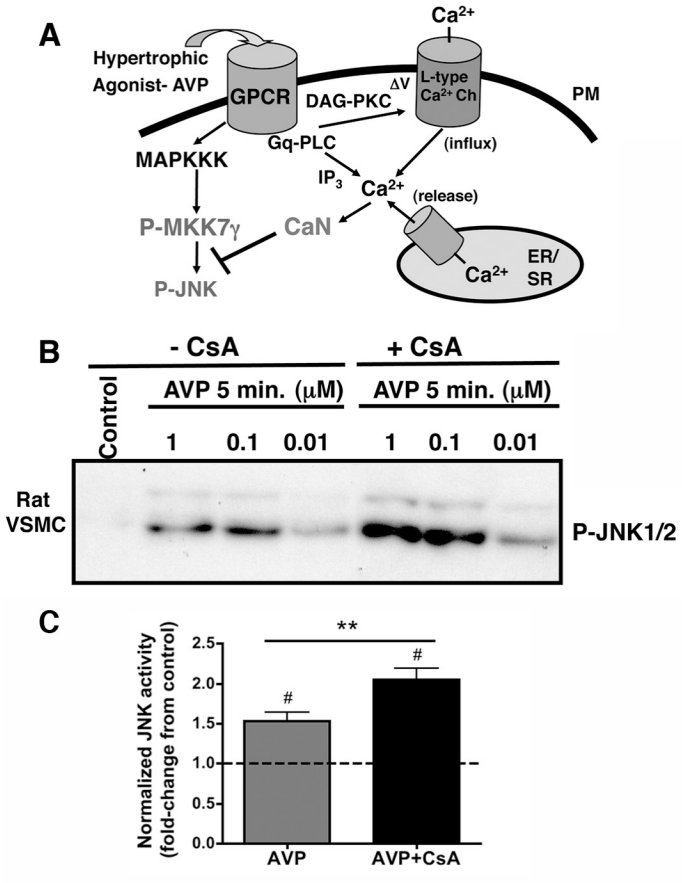

Figure 10